OFFICE OF NAVAL RESEARCH

GRANT: N00014-93-0545

R & T CODE: 413V005

Technical report # 5

THE KINETICS OF FORMATION AND DISSOLUTION OF CONDENSED COUMARIN FILMS

by

T. Wandlowski and R. de Levie

prepared for publication in the Budevski Festschrift
of the Bulgarian Chemical Communications

Chemistry Department, Georgetown
University, Washington DC 20057

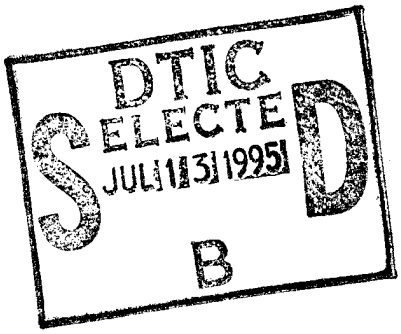

June 26, 1995

REPORT DOCUMENTATION PAGE

Form Approved
OMB No. 0704-0188

1. AGENCY USE ONLY (*Leave blank*)	2. REPORT DATE	3. REPORT TYPE AND DATES COVERED
	June 26, 1995	Technical

4. TITLE AND SUBTITLE

THE KINETICS OF FORMATION AND DISSOLUTION OF CONDENSED COUMARIN FILMS

5. FUNDING NUMBERS

N00014-93-1-0545

6. AUTHOR(S)

T. Wandlowski and R. de Levie

7. PERFORMING ORGANIZATION NAME(S) AND ADDRESS(ES)

Chemistry Department, Georgetown University, Washington DC

8. PERFORMING ORGANIZATION REPORT NUMBER

Technical report #5

9. SPONSORING/MONITORING AGENCY NAME(S) AND ADDRESS(ES)

Office of Naval Research, Dept. of the Navy, Arlington VA 22217

10. SPONSORING/MONITORING AGENCY REPORT NUMBER

11. SUPPLEMENTAL NOTES

12a. DISTRIBUTION AVAILABILITY STATEMENT

Approved for public release; distribution unlimited

12b. DISTRIBUTION CODE

13. ABSTRACT (*Maximum 200 words*)

Following stochastic nucleation, the resulting capacitance change is used to trigger a change in the applied potential in order to study growth and dissolution at potentials which are otherwise difficult to access. Experimental results show that the dissolution rate depends on the age of the compact film.

By using simultaneous measurements of current-time and capacitance-time curves under circumstances where film formation is stochastic, the possible origin of some so far unexplained maxima on polarographic current-time curves reported in the literature has been identified. These reflect charging currents accompanying the formation of condensed films

14. SUBJECT TERMS

Coumarin condensation
Polarographic maxima

15. NUMBER OF PAGES

34

16. PRICE CODE

17. SECURITY CLASSIFICATION OF REPORT	18. SECURITY CLASSIFICATION OF THIS PAGE	18. SECURITY CLASSIFICATION OF ABSTRACT	20. LIMITATION OF ABSTRACT
Unclassified	Unclassified	Unclassified	Unlimited

THE KINETICS OF FORMATION AND DISSOLUTION OF CONDENSED COUMARIN FILMS

Thomas Wandlowski & Robert de Levie
Chemistry Department, Georgetown
University, Washington DC 20057 USA

Abstract

Following stochastic nucleation, the resulting capacitance change is used to trigger a change in applied potential in order to study growth and dissolution at potentials which are otherwise difficult to access. Experimental results show that the dissolution rate depends on the age of the compact film.

By using simultaneous measurements of current-time and capacitance-time curves under circumstances where film formation is stochastic, the possible origin of some so far unexplained maxima on polarographic current-time curves reported in the literature has been identified . These maxima may reflect charging currents accompanying the formation of condensed films.

Introduction

The adsorption of coumarin (2H-1-benzopyran-2-one) has already been studied extensively [1-13]. Laitinen & Mozier [1] were the first to report its strong adsorption. Griffiths & Westmore [2,3] concluded from drop time measurements that coumarin is adsorbed with its molecular plane parallel to the interface. Partridge et al. [4] subsequently inferred that coumarin adsorbs at the mercury-water interface in two different orientations, depending on the applied potential. At the most positive potentials, coumarin adsorption reaches a value of about 3.1 μmoles m^{-2}, which has been interpreted as corresponding with a "planar" orientation [4], i.e., with the plane through the coumarin parallel to that of the interface, or with an "inclined" one [6]. In accordance with the notation used by Thomas et al. [11], we will denote coumarin adsorption in this region as state I.

Dedicated to Prof. Evgeni Budevski on the occasion of his 70th birthday.

At more negative potentials and sufficiently large coumarin concentrations, the capacitance is much lower, and the maximum value of the interfacial excess is reported as 6.1_5 μmoles m^{-2} [4]. Coumarin is here believed to be oriented with its molecular plane normal to the interface, presumably oriented primarily by its dipole moment [4], perhaps with its carbon atoms C(4) and C(5), or C(5) and C(6), closest to the electrode [11]. Thomas et al. denoted this type of coumarin adsorption as state III. In between states I and III, there is a pronounced capacitance peak [6], apparently associated with the reorientation of adsorbed coumarin molecules. Extensive further studies of coumarin adsorption, and of the corresponding inhibition of faradaic processes, have been reported by Moussa, Ghaly, Abou-Romia and coworkers [7-10].

Thomas et al. [11] and Srinivasan & de Levie [12] reported the formation of a compact film, and stochastic behavior in the formation of this compact film. Thomas et al. [11] labeled this compact film, situated between regions III and IV, as layer II, and assumed that it corresponds to a molecular orientation in which the coumarin carbons C(6) and C(7) point towards the metal. Srinivasan & de Levie [13] reported further stochastic aspects of coumarin adsorption. This topic has continued to intrigue us, since this is the only system known so far where the stochastics of nucleation can be studied on full-sized, spherical mercury drops.

In the present communication we report some additional results on coumarin compact films. These measurements were initiated in order to understand several puzzling, seemingly unrelated observations reported in the literature [14-19], a topic to which we will return at the end of this communication. However, before that, we will show how the nature of the nucleation of coumarin films changes as a function of the applied potential, and report on some time-dependent properties of such films, as deduced from desorption transients.

For reference we show, in Fig. 1 the interfacial capacitance of mercury in contact with aqueous 0.5 M NaF + 5 mM coumarin at 5^{o}C, as measured on a hanging mercury electrode at a scan rate of 5 mV s^{-1}. The figure identifies the regions I, II and III and clearly shows the pronounced hysteresis between the transitions I $\rightleftarrows$ II and II $\rightleftarrows$ III.

Fig. 1

Experimental procedures

Most measurements used hanging mercury droplets of three surface areas, 1.11_1, 1.60_5 and 2.40_7 mm^2 respectively, made with a PAR 303 mercury dispenser. Polarographic measurements were made with a dropping mercury electrode with a mercury flow rate of 0.6 mg s^{-1} and a drop time of 15.3 s at open circuit. An external saturated calomel electrode, connected via a salt bridge, was used. All potentials are referred to this SCE. All measurements were made at 5.0 ± 0.2 °C.

The solutions were made from pyrodistilled water, NaF (Merck Suprapur), $[Co(NH_3]_2(SO_4)_3$ (a gift from Prof. J. Earley of this department) and 5 mM coumarin (Alpha Inorganics, recrystallized and vacuum-sublimed). All supporting electrolyte solutions were treated with activated charcoal. Nitrogen was used to deaerate the solutions before each measurement.

Capacitance measurements were made with a 1.59 kHz sine wave of 2.5 mV amplitude, superimposed on a voltage ramp or step. Positive feedback just short of oscillatory instability was used to compensate for the solution resistance. The alternating current was amplified, phase-selectively rectified with a lock-in amplifier, digitized, and stored in a 80286-based computer. In our double potential step experiments we used a D-400 window discriminator from Mike Walsh Electronics. In some experiments, the ac and dc signals were recorded simultaneously.

The kinetics of formation of the compact film

Capacitance transients were measured following single potential steps from an initial potential E_0 in region I to potentials E_1 inside region II. At sufficiently high coumarin concentrations ($\geq$ 2 mM) so that diffusion is not a rate-determining factor, neither the value of E_0 nor the residence time at that potential affect the subsequent capacitance transients. In 0.5 M NaF + 5 mM coumarin, deterministic capacitance transients were obtained for $E_1 \leq -0.555$ V, as illustrated in Fig. 2. At more negative potentials, film condensation becomes too fast to be resolved with our present equipment.

Fig. 2

Analysis of such transients was based on the fractional film coverage

$$\Theta = \frac{C_i - C}{C_i - C_f} \qquad (1)$$

where C_i and C_f are the *i*nitial and *f*inal capacitance (i.e., the capacitance at the beginning and end of the transient) respectively, while C is its value during the transient, as a function of time t. From Θ we then calculated the extended fractional coverage

$$\Theta_x = -\ln(1-\Theta) = \ln\frac{C_i - C_f}{C - C_f} \qquad (2)$$

Avrami plots of $\ln \Theta_x$ versus $\ln t$ yielded slopes of 3.07 ± 0.2 , indicating so-called progressive nucleation plus two-dimensional growth as the rate-limiting processes. We are here clearly in the regime of deterministic nucleation.

When the final potential E_1 in the single step experiment is chosen in the range from -0.530 to -0.555 V, stochastic behavior is encountered. Fig. 3 illustrates this with a number of capacitance transients obtained under identical experimental conditions at E_1 = -0.540 V. All capacitance traces exhibit the same values for C_i and C_f , but there is stochasticity in the onset of each transient as well as its shape. The hanging drop is essentially spherical and, therefore, isotropic, so that single nucleations and subsequent growths give rise to identical capacitance transients, regardless of the precise location of the nucleation. The observed differences between the individual capacitance transients (apart from their different starting times) are therefore indicative of multiple nucleations. Consequently we are here in the domain of so-called oligonucleation.

Fig. 3

By selecting E_1 to be larger than -0.530 V, we reach the domain of mononucleation, in which nucleation is so slow that there is only a negligible chance of a second nucleation during the time it takes the first nucleus to form a complete film. Some corresponding capacitance transients are shown in Fig. 4(a).

Fig. 4

For an isotropic sphere, the growth of a compact film once it has been nucleated is given by [20]

$$2\Theta = 1 - \cos[v_g(t-t_0)/r] \qquad (3)$$

where v_g is a linear growth velocity, t_0 is the moment of nucleation, and r is the radius of the mercury droplet. Consequently, a plot of arccos (1-2Θ) versus t is linear, with a slope v_g/r and intercept t_0 . Such plots are shown in Fig. 4(b). Experiments with drops of three different sizes yield v_g = 7.5 ± 0.3, 7.6 ± 0.2 and 7.5 ± 0.2 mm s^{-1} for small, medium and large drops respectively, clearly demonstrating that the growth rate constant v_g is independent of drop size. These data were obtained by analyzing 50 individual capacitance transients for each drop size.

There is a charging current associated with such capacitance transients. Let the charge density be Q_0 of the fraction of the electrode not yet covered by the compact film, while the charge density of the covered fraction is Q_1 . The total interfacial charge q is then $4\pi r^2 [Q_0(1-\Theta)+Q_1\Theta]$, so that the charging current i_c follows from eqn. (3) as

$$i_c = dq/dt = 4\pi r^2 \Delta Q \; d\Theta/dt = 2\pi r \Delta Q \; v_g \sin [v_g(t-t_0)/r] \qquad (4)$$

where $\Delta Q = Q_0 - Q_1$. Fig 5 shows charging currents, measured simultaneously with the capacitance transients of Fig. 4a. Analysis of such current transients in terms of eqn. (4) leads to an experimentally independent estimate of the growth velocity v_g. As can be seen from the numerical values listed in the legend of Fig. 5, both approaches provide fully equivalent results.

Fig. 5

The dependence of the linear growth velocity v_g on potential was measured for -0.490 V > E_1 > -0.525 V, and the results are summarized in Fig. 6. It was verified that these values are, within the limits of experimental error, independent of drop size.

Fig. 6

The hysteresis loop in Fig. 1 indicates that the compact film, once formed, is stable at potentials negative of about -0.430 V, yet the nucleation rate at that potential is too small to observe capacitance transients following single potential steps within times of the order of 10 s. When much longer observational times must be used, impurity accumulation at the interface can interfere with the nucleation process, and may thereby further decrease the already low nucleation rate. We have therefore used a modified double potential step procedure, in which E_1 is selected in the region of mononucleation. After the first step in potential, the capacitance goes to the metastable state shown in Fig. 4. At some later time (unpredictably because of the stochasticity of the nucleation), the

capacitance then will start to descend to the pit capacitance. When, during this descent, the capacitance passes a preset value, roughly corresponding to $C = \frac{1}{2}(C_i + C_f)$ (at which point about half of the electrode surface is covered by the compact film), a Schmitt trigger initiates the second step in potential, to the more positive value E_2, where we can then observe further, slower film growth, or even film dissolution. Fig. 7 shows the capacitance transients following the transition $E_1 \rightarrow E_2$.

Fig. 7

Instead of eqn. (3) we now have

$$2\Theta = 1 - \cos [v_{g1}t_1/r + v_{g2}(t-t_1)/r] \qquad (5)$$

where t_1 denotes the time at which the potential is changed from E_1 to E_2, and v_{g1} and v_{g2} are the linear growth velocities at the potentials E_1 and E_2, i.e., for $t_0 \leq t \leq t_1$ and $t \geq t_1$ respectively. It is clear that continued growth fits the above description, and allows us to determine the linear growth velocity v_g at potentials with negligible nucleation rates. In order to verify the validity of the above approach, measurements were made at three different values of r, the radius of the mercury droplet. Fig. 7 also shows, as drawn lines, the curves reconstituted with the parameters obtained from the non-linear least-squares analyses based on eqn. (5). These curves are, by and large, indistinguishable from the experimental points. The linear growth velocity v_g is indeed found to be constant within the limits of experimental uncertainty.

With the aid of eqns. (1) and (3), we can also express $1-2\Theta$ and $v_{g1}t_1/r$ in terms of the capacitance, in which case eqn. (5) becomes

$$\arccos\frac{2C-C_i-C_f}{C_i-C_f} - \arccos\frac{2C_1-C_i-C_f}{C_i-C_f} = \frac{v_{g2}(t-t_1)}{r} \qquad (6)$$

where C_1 is the capacitance at $t=t_1$. Consequently a plot of the left-hand side of eqn. (6) versus $(t-t_1)$ should yield a straight line with slope v_{g2}/r. Unfortunately, the precise experimental determination of C_1 is difficult, which is why we have tested eqn. (5) rather than eqn. (6).

We have already described in detail in an earlier communication [12] how, based on the work of Obretanov et al. [21], one can obtain the *nucleation* velocity from an analysis of *growth* transients following single potential steps in the region of mononucleation. In short, extrapolations of growth curves yield the moments of nucleation, t_0. When these are sorted in bins they provide the probability P_0 that nucleation has not yet occurred in a given time interval Δt. A plot of $-\ln P_0$ as a function of time t then produces a plot from which both the induction time and the steady-state nucleation rate can be read. Figs. 8 and 9 illustrate this procedure.

Figs. 8,9

We again ask the question: what is the dependence of the nucleation rate on drop radius. The three curves shown in Fig. 9a display the resulting data for different drop radii. They show a non-zero initial slope which, as before, we ascribe to steady-state nucleation at the lumen of the capillary. Since all measurements were made with the same capillary, the latter should be independent of drop size. Moreover, for two independent Poisson processes, the resultant rates are the algebraic sum of the rates of the individual processes [22]. We can therefore correct the data by estimating the initial slope in the plot of $-\ln P_0$ vs. t, and by subtracting this from all three curves. The resulting, corrected curves are shown in Fig. 9b. Their steady-state slopes yield relatively constant nucleation rate parameters of 39, 42.5 and 44 $m^{-2}\ s^{-1}$ for the three drop areas, where the latter vary by more than a factor of two. The dependence of the nucleation rate on the applied potential is illustrated in Fig. 9c, and Fig. 5 incorporates the resulting nucleation velocities. Thomas et al. mentioned that, in their measurements, nucleation occurred only at the lumen of their capillary [11]; our present results are more akin to those of Srinivasan and de Levie [12], in that only a relatively small fraction of the observed nucleations appear to originate at that lumen.

Finally we briefly address a different question, namely that of the dependence of the nucleation rate on concentration. Since two-dimensional nucleation and growth occur in a direction perpendicular to the applied electric field, their dependence on potential must be an indirect one, through the effect of potential on the interfacial concentration. Since we don't know the latter, we have so far listed rates v rather than rate constants k for nucleation and growth. However, the quantitative agreement of the experimental growth transients with eqns. (3) through (5) give us confidence that the growth rate is a simple first-order process, i.e., directly proportional to the concentration c of the incorporating species, so that $v_g = k_g c$. Assuming this to be true, we can determine the dependence of the nucleation rate on concentration c simply by plotting $\ln v_n$ versus $\ln v_g$ over the range of potentials where we have data for both. We note here that this range of potentials is at least 70 mV from the pit edge, hence growth can be considered a unidirectional, irreversible process, so that the rate of dissolution need not be taken into account. Figure 10 shows such an analysis, and yields a slope of the order of 4. Unfortunately, there is only a very narrow interval, of about 20 mV, over which mononucleation can be observed.

Fig. 10

The kinetics of dissolution of the compact film

Single potential steps, starting from -1.000 V (i.e., in the capacitance pit region II), and stepping to potentials where that film is not stable, yield capacitance transients which are often S-shaped and deviate markedly from a single exponential, see Fig. 11a, as already reported [12]. As can be seen in Fig. 11b, the age of the compact film at the time of the potential step affects the dissolution transients. The longer the potential resides in the compact film region, the slower the dissolution transient, and the more it appears to require a nucleation event. Apparently the film anneals, i.e., some of the domain boundaries disappear.

Fig. 11

Similar experiments starting from -0.52 V show that the potential at which the film is formed does not change the dissolution transients much for a waiting time of 5 seconds after the film has formed (which, at -0.52 V, is a stochastic event), see Fig. 12a. However, the aging effect now is different: at longer film ages, the capacitance transients exhibit at least two processes with different time constants, see Fig. 12b. These transients suggest that there is an initial process, which depends on the initial potential E_0, and brings the capacitance to an intermediate value, followed by a second process which, at a speed essentially independent of E_0 , lifts the capacitance to its final value. The latter process may well be associated with the interfacial reorientation believed to occur at those final potentials.

Fig. 12

Double potential step experiments show this even more clearly, see Fig. 13. (We do not understand why the capacitive transients following single and double potential step experiments are so different.) Fig. 13 indicates that the transients showing two successive steps cannot be explained in terms of a difference between mononucleation and polynucleation, i.e., through the possible formation of domain boundaries in polynucleation, because qualitatively similar behavior is observed at -0.52 V, -0.6 V and -0.7 V. At present, the only conclusion we can draw from these observations is that the dissolution transients starting from potentials near the positive pit edge are clearly more complicated than simple reverse growth curves.

Fig. 13

Finally we note that the second process showing in these dissolution transients cannot be resolved any more in the capacitance transients as the temperature is raised to above 25°C for Hg in contact with an aqueous solution of 0.5 M NaF + 5 mM coumarin.

Polarographic effects

As indicated in the introduction, the stimulus for the present study were several reports in the literature of unusual peaks on polarographic current-time curves. In all cases, these appeared when the faradaic process was suppressed by the time-dependent formation of an adsorbate film, such as made by tribenzylamine [14,15] or alkyltriphenylphosphonium bromide [16-19]. In these cases, the initial part of the drop-time curves is uninhibited. Subsequently, inhibition sets in, apparently due to diffusion-related accumulation of the adsorbate at the mercury-solution interface, and the current drops. Then follows a shortlived current peak, sometimes followed by one or more steps in the current, which finally bring it to its most inhibited level. Some of these steps are likely to reflect various intermediate molecular organizations in the formation of a compact film at the interface. There is, however, another effect which may be involved, viz. the capacitance current associated with the formation of a compact film, and it is this aspect which we will illustrate below.

Phase transitions are often associated with rather abrupt changes in interfacial capacitance. Because of the magnitude of the charging currents involved, such changes in capacitance are often observable in a polarographic experiment, as a charging current i_c directly proportional to dC/dt. We already illustrated such charging current peaks in Fig. 5.

Figure 14 shows current-time curves for the polarographic reduction of hexaminecobaltate in the absence and presence of coumarin. Because the coumarin concentration is sufficiently high, inhibition by adsorbed coumarin starts at the very beginning of drop life. Then the current drops to essentially zero, a transition which is associated with a sharp current peak, as is best seen in Fig. 14b. The transitions in this case are stochastic, and the peak areas are proportional to the areas of the drop at the moment of compact film formation, i.e., to $t^{2/3}$. In this case, the stochasticity of the phenomenon clearly shows that these peaks are associated directly with the nucleation process, i.e., with the formation of a compact film. Clearly, such charging current peaks should be considered when trying

to interpret the complex behaviors observed in polarographic current-time curves involving inhibitors. In cases where the adsorbate concentration is lower, so that adsorption is initially diffusion-controlled, one would expect polarographic current-voltage curves in which there is an initial, gradually increasing inhibition resulting from diffusion-controlled adsorption, followed by the more abrupt formation of a compact film, with an associated charging current peak.

Fig. 14

Acknowledgements

We are grateful to Prof. Eagles of the Georgetown University Biology Department for the loan of a the window discriminator, and to the Office of Naval Research for financial support through grant N00014-93-1-0545.

References

1. H. Laitinen & Mozier, J. Am. Chem. Soc. 80 (1958) 2363.
2. V. S. Griffiths & J. B. Westmore, J. Chem. Soc. (1962) 1704.
3. V. S. Griffiths & J. B. Westmore, J. Chem. Soc. (1963) 4941.
4. L. K. Partridge, A. C. Tansley & A. C. Porter, Electrochim. Acta 11 (1966) 517.
5. L. K. Partridge, A. C. Tansley & A. C. Porter, Electrochim. Acta 14 (1969) 223.
6. B. B. Damaskin, S. L. Dyatkina & S. I. Petrochenko, Elektrokhim. 5 (1969) 935.
7. A. A. Moussa, H. A. Ghaly & M. M. Abou-Romia, Electrochim. Acta 20 (1975) 485.
8. A. A. Moussa, H. A. Ghaly, M. M. Abou-Romia & F. El-Taib Heakal, Electrochim. Acta 20 (1975) 489.
9. H. A. Ghaly, A. M. Bekheet & A. A. Mazhar, Electrochim. Acta 27 (1982) 595.
10. M. M. Abou-Romia, A. A. Mazhar & A. M. Bekheet, Electrochim. Acta 28 (1983) 1481.
11. G. Thomas, C. Buess-Herman & L. Gierst, J. Electroanal. Chem. 214 (1986) 597.
12. R. Srinivasan & R. de Levie, J. Phys. Chem. 91 (1987) 2904.
13. R. Srinivasan & R. de Levie, J. Electroanal. Chem. 249 (1988) 321.
14. J. Kůta & I. Smoler, Coll. Czech. Chem. Comm. 27 (1962) 2349.
15. J. Kůta & I. Smoler, Coll. Czech. Chem. Comm. 32 (1967) 2691.
16. E. Müller, H. Matschiner & H.-D. Dörfler, Z. Phys. Chem. 260 (1979) 804.
17. H.-D. Dörfler & E. Müller, J. Electroanal. Chem. 105 (1979) 383.
18. H.-D. Dörfler & E. Müller, J. Electroanal. Chem. 121 (1981) 153.
19. A. Anastopoulos & A. Christodoulou, Coll. Czech. Chem. Comm. 53 (1988) 732.
20. L. Gierst, C. Franck, G. Quarin & C. Buess-Herman, J. Electroanal. Chem. 129 (1981) 353.
21. W. Obretenov, V. Bostanov & V. Popov, J. Electroanal. Chem. 132 (1982) 273.
22. R. Sridharan & R. de Levie, J. Electroanal. Chem. 218 (1987) 287.

Figure legends

Fig. 1. The interfacial capacitance of mercury in contact with aqueous 0.5 M NaF (curve 1) and the same in the presence of 5 mM coumarin (curves 2 and 2′). Temperature 5^0C, measuring frequency 1.59 kHz, amplitude 2.5 mV, scan rate -5 mV s^{-1} (data points) and +5 mV s^{-1} (broken line). Open circles show the initial capacitance C_i observed immediately after stepping the potential from region I into region III, cf., Fig. 2.

Fig. 2. Triplicate measurements of the interfacial capacitance of mercury in contact with aqueous 0.5 M NaF + 5 mM coumarin as a function of time following a single potential step from E_0 = -0.400 V to E_1 = -0.560 V (curve 1); -0.565 V (curve 2); and -0.570 V (curve 3). These transients are deterministic, i.e., they are reproducible from one experiment to the next. Temperature 5^oC, electrode area 2.41 mm^2. The solid lines were calculated by non-linear least-squares fitting to $\Theta = 1-\exp[-(bt)^m]$, which yielded the parameters b = (35±20) s^{-1}, m = 3.20±0.07 (curve 1); b = (59±36) s^{-1}, m = 3.05±0.06 (curve 2), and b = (82±61) s^{-1}, m = 3.05±0.09 (curve 3). The inset shows the corresponding Avrami plots for one transient at each potential.

Fig. 3. Some capacitance transients as in Fig. 2, except that E_1 = -0.540 V. The transients are now stochastic; the numbers indicate their sequence number in a set of 50 repeat experiments. The solid line through curve # 37 was calculated with eqn. (3), v_g/r = 27.23 s^{-1} and t_0 = 0.100 s. Similar curves but with other values for t_0 fit through curves # 5, #44 and #29, but would poorly fit curves # 23 and #20, which clearly involve multiple nuclei.

Fig. 4a. Some capacitance transients as in Fig. 2 except that E_1 = -0.520 V. Now all transients reflect mononucleation, i.e., they can all be represented by eqn. (3)

Fig. 4b. Analysis of the linear dependence of arccos $(1-2\Theta)$ on $(t-t_0)$ for six transients each on small (curve 1), medium (curve 2) and large (curve 3) drops respectively. The values for t_0 were determined by non-linear least-squares analysis of the individual transients. Lines are drawn with v_g/r = 17.2 s^{-1}.

Fig. 5. Current-time transients recorded simultaneously with the capacitance transients of Fig. 4a. The lines were drawn using eqn.(4) with $v_g/r = 17.5\ s^{-1}$, Δq = 108 nC, and appropriate values for t_0 , as obtained from non-linear least-squares fits to 50 repeat measurements of current transients shown such as shown here.

Fig. 6. The growth rates v_g (use left-hand scale) and nucleation rates v_n (use the right-hand scale) as a function of the applied potential, for Hg in contact with aqueous 0.5 M NaF + 5 mM coumarin at 5°C. Results for v_g are shown for three drop radii: r = 0.297 mm (small open circles), r = 0.357 mm (medium-sized open circles) and r = 0.457 mm (large open circles). Growth rates from double-step experiments, at potentials between -0.430 and -0.480 V vs. SCE, are identified by a central point inside the circle. Solid circles are data obtained in the presence of 5 mM $[Co(NH_3]_2(SO_4)_3$.

Fig. 7. Capacitance transients following a double step potential, first from E_0 = -0.400 V to E_1 = -0.510 V and, after mononucleation and partial film formation, to E_2 = -0.460 V (curve 1), -0.455 V (curve 2), -0.450 V (curve 3), -0.445 V (curve 4), -0.441 V (curve 5), -0.436 V (curve 6), -0.432 V (curve 7), -0.428 V (curve 8), -0.425 V (curve 9) and -0.422 V (curve 10). The thin lines show curves calculated with equation (6) using the following numerical values: t_1 = 0.359 ± 0.003 s, $v_g/r = 4.00 \pm 0.03\ s^{-1}$ (curve 1); t_1 = 0.532 ± 0.004 s, $v_g/r = 2.72 \pm 0.02\ s^{-1}$ (curve 2); t_1 = 0.692 ± 0.004 s, $v_g/r = 2.08 \pm 0.01\ s^{-1}$ (curve 3); t_1 = 0.962 ± 0.005 s, $v_g/r = 1.48 \pm 0.01\ s^{-1}$ (curve 4); t_1 = 1.386 ± 0.006 s, $v_g/r = 41.01 \pm 0.01\ s^{-1}$ (curve 5), and t_1 = 2.295 ± 0.013 s, $v_g/r = 0.61 \pm 0.01\ s^{-1}$ (curve 6).

Fig. 8. Nomogram showing the number of measurements (out of a total of 550) at which the nucleation started in a given time interval (of 25 ms width) after application of a single step in potential, from E_0 = -0.400 V to E_1 = -520 V.

Fig. 9. (a): Plot of -ln P_o versus time t elapsed after a single step in potential, from E_0 = -0.400 V to E_1 = -520 V, obtained with three different drop sizes: small (curve 1), medium (curve 2) and large (curve 3). Each curve results from at least 200 individual measurements. P_o represents the probability that no nucleus has yet formed on a given mercury droplet. (b): The same data after subtraction of the estimated contribution due to nucleations originating at the lumen of the capillary. (c): The same as under (b) but for the largest drop size, and E_1 = -0.505 V (curve 1); -0.510 V (curve 2); -0.515 V (curve 3); -0.520 V (curve 4), and -0.525 V (curve 5).

Fig. 10. Double-logarithmic plot of the steady-state nucleation rate v_n versus the growth rate v_g , indicating the dependence of the nucleation rate on the concentration of the incorporating species. The data used are the same as shown in Fig. 5 for large mercury drops in the absence of cobalt hexammine sulfate, at potentials from -0.505 to -0.525 V vs SCE. The line drawn is obtained by least-squares fit, with a slope of 4.10 .

Fig. 11. (a): Capacitance transients following a single potential step from E_0 = -1.000 V (i.e., inside the capacitance pit region III) at t_0 = 5 s to E_1 = -0.4260 V (curve 1), -0.4265 V (curve 2), -0.4270 V (curve 3), -0.4275 V (curve 4), -0.4280 V (curve 5) and -0.4285 V (curve 6). (b): The effect of varying the age t_0 of the film before the potential is stepped to -0.4265 V; the times spent at E_0 are 2.5 s (curve 1), 5.0 s (curve 2), 10 s (curve 3), 20 s (curve 4) and 50 s (curve 5). Conditions for a and b: Hg in contact with 0.5 M aqueous NaF + 5 mM coumarin at 5.0°C.

Fig. 12. (a): Capacitance transients following a single potential step from E_0 = -0.520 V (i.e., inside the capacitance pit region III) at t_0 = 5 s to E_1 = -0.4260 V (curve 1), -0.4265 V (curve 2), -0.4270 V (curve 3), -0.4275 V (curve 4), -0.4280 V (curve 5) and -0.4285 V (curve 6). (b): The effect of varying the age t_0 of the film before the potential is stepped to -0.4265 V; the times spent at E_0 are 2.5 s (curve 1), 5.0 s (curve 2), 10 s (curve 3), 20 s (curve 4) and 50 s (curve 5). Conditions for a and b: Hg in contact with 0.5 M aqueous NAF + 5 mM coumarin at 5.0°C.

Fig. 13. Capacitance transients following double potential steps from E_0 = -0.300 V for 5.0 s to E_1 for 5 s and, finally, to E_2 = -0.4265 V. The transients shown are recorded starting at the transition $E_1 \rightarrow E_2$. The various curves are for E_1 = -0.52 V (curve 1), -0.6 V (curve 2), -0.7 V (curve 3), -0.8 V (curve 4), -0.9 V (curve 5) and -0.1 V (curve 6). Conditions: Hg in contact with 0.5 M aqueous NAF + 5 mM coumarin at 5.0°C.

Fig. 14. (a): Current-time curves for the polarographic reduction of 5 mM $[Co(NH_3]_2(SO_4)_3$ in aqueous 0.5 M NaF at 5°C at -0.520 V ion the absence (curve 1) and presence (curves 2 through 6) of 5 mM coumarin. The current-time curves in the presence of coumarin first show partial inhibition, which becomes essentially complete inhibition upon the stochastic formation of a compact film. At that transition, the current shows a sharp peak before dropping to almost zero. Thin lines have been added to the data to connect the few points during these transitions. (b): Enlarged portions of three of the current peaks associated with the stochastic formation of coumarin films. The current transients have been moved by an arbitrary time t_0 to get them all on one record at his scale.

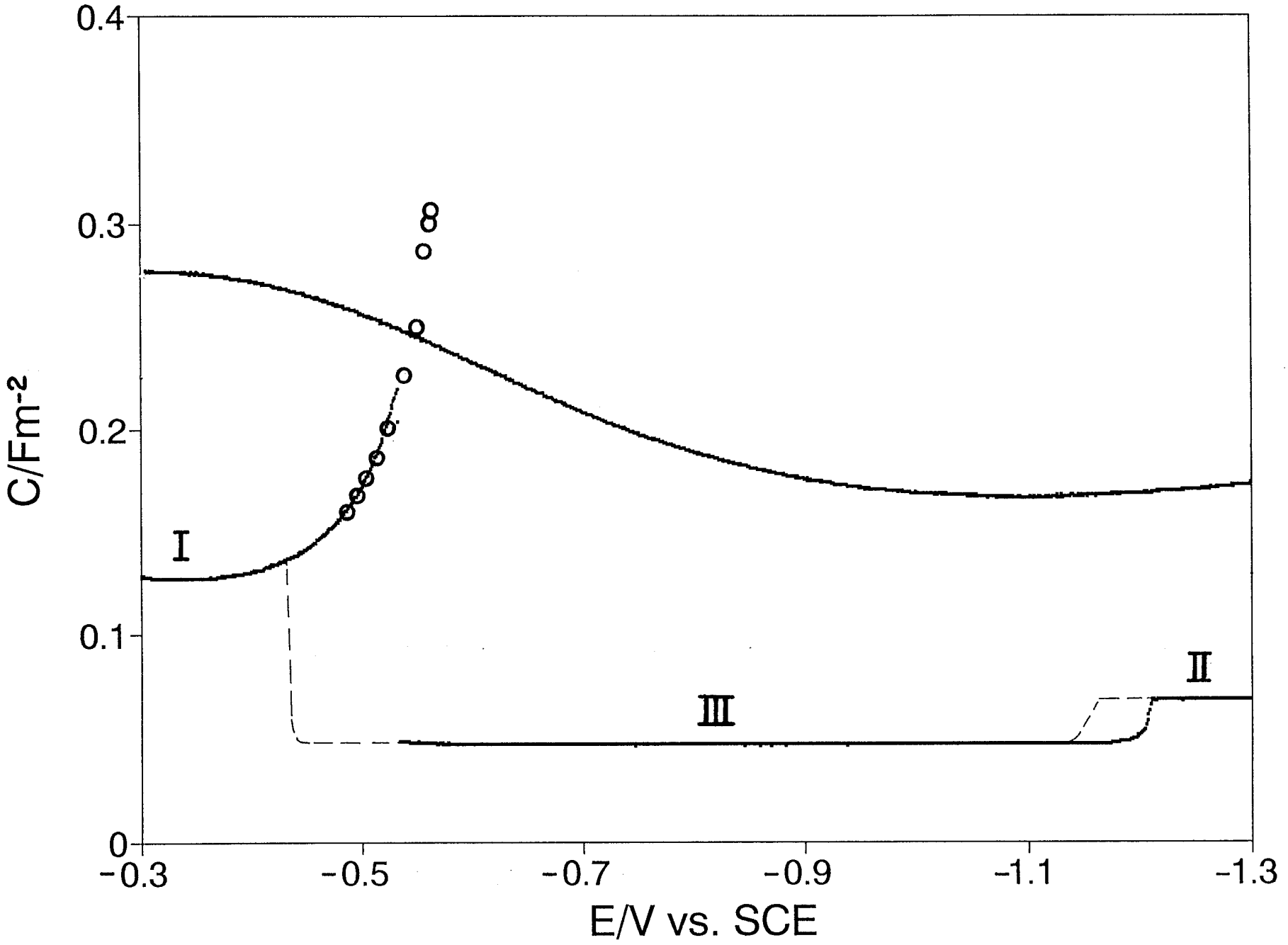

FIG. 1

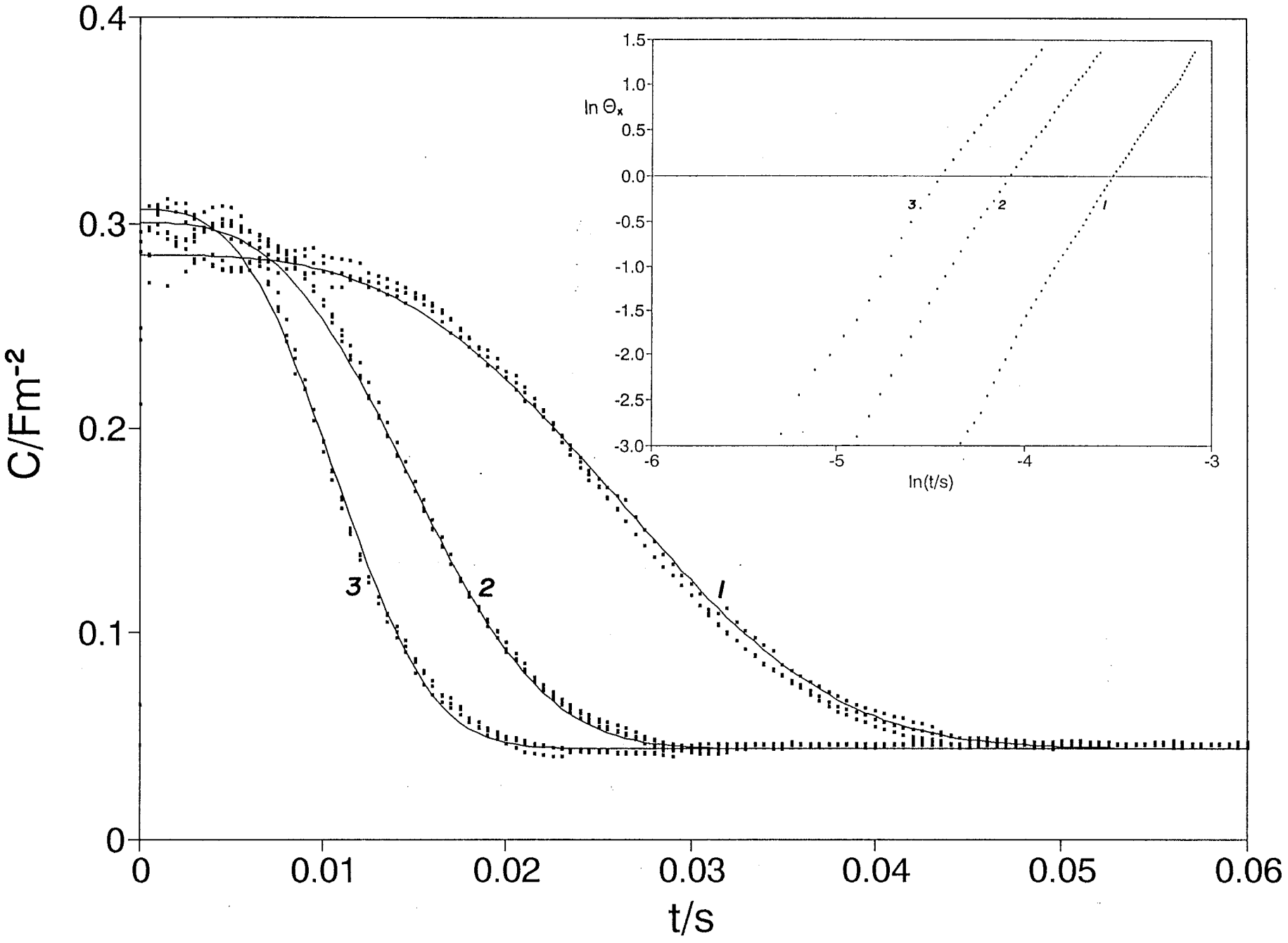
0.4
0.3
0.2
0.1
0
C/Fm-2
0
0.01
0.02
0.03
0.04
0.05
0.06
t/s
1
2
3
1.5
1.0
0.5
0.0
-0.5
-1.0
-1.5
-2.0
-2.5
-3.0
ln Θx
-6
-5
-4
-3
ln(t/s)

FIG 2

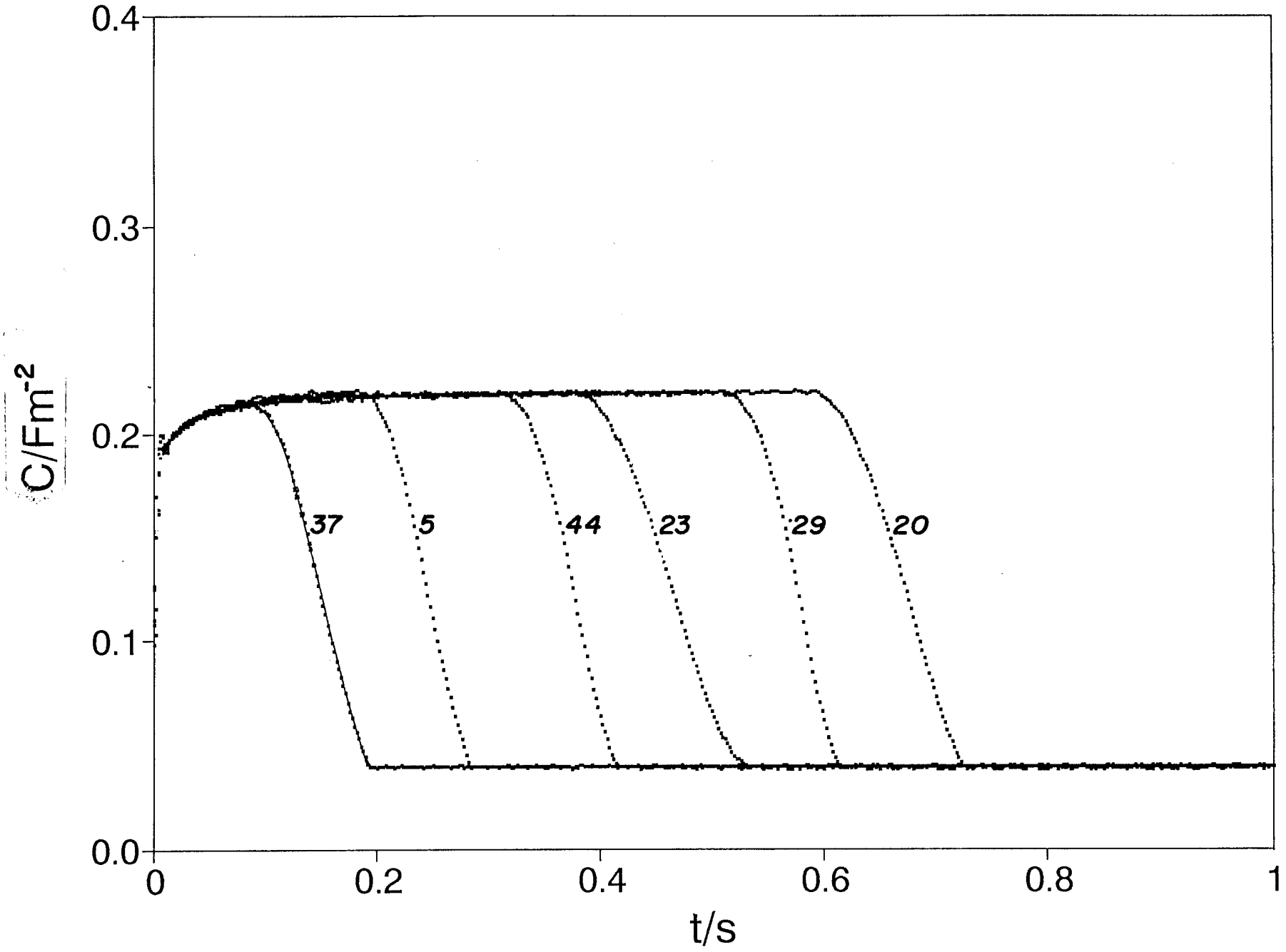

FIG. 3

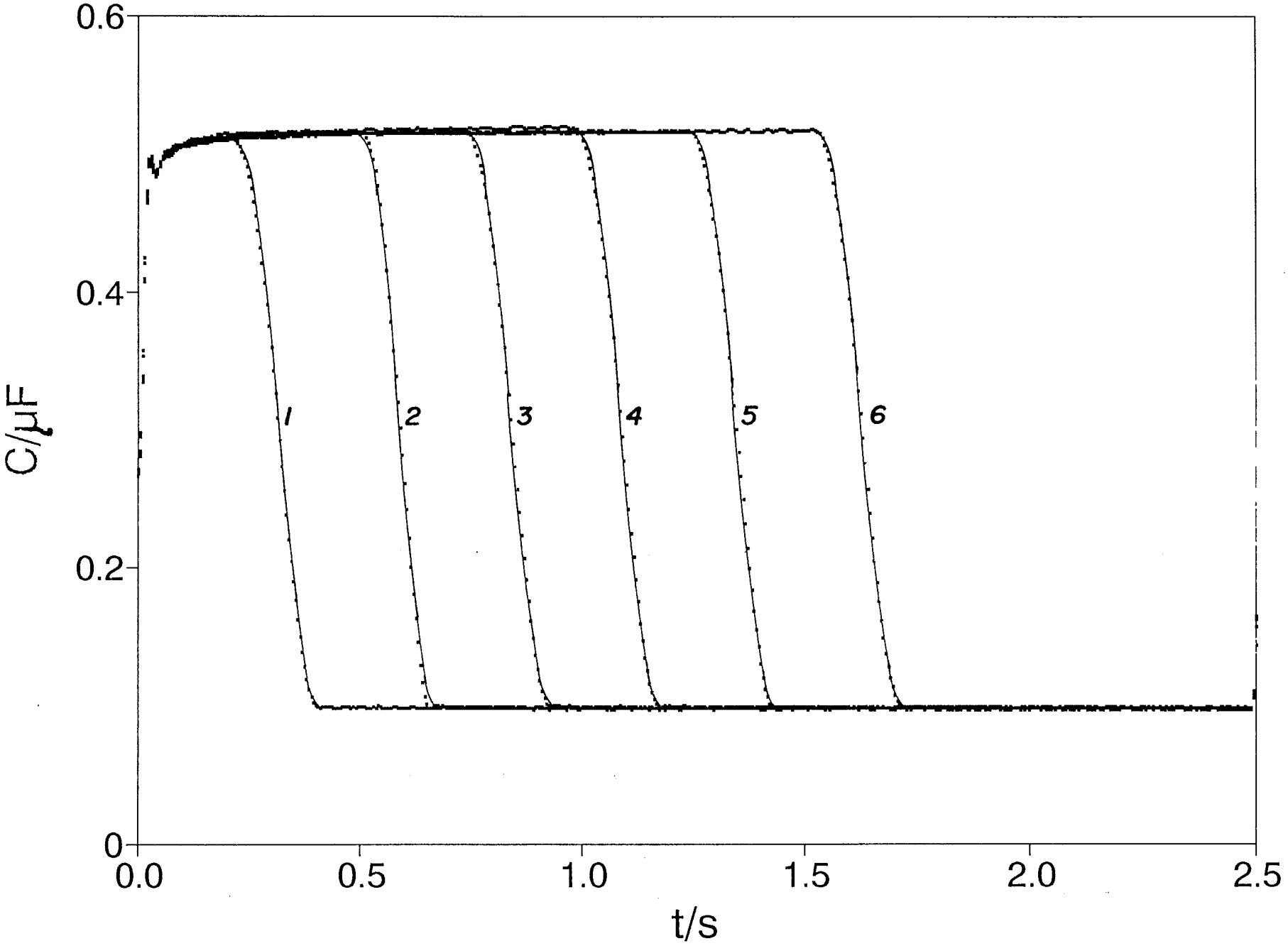

Fig. 4(a)

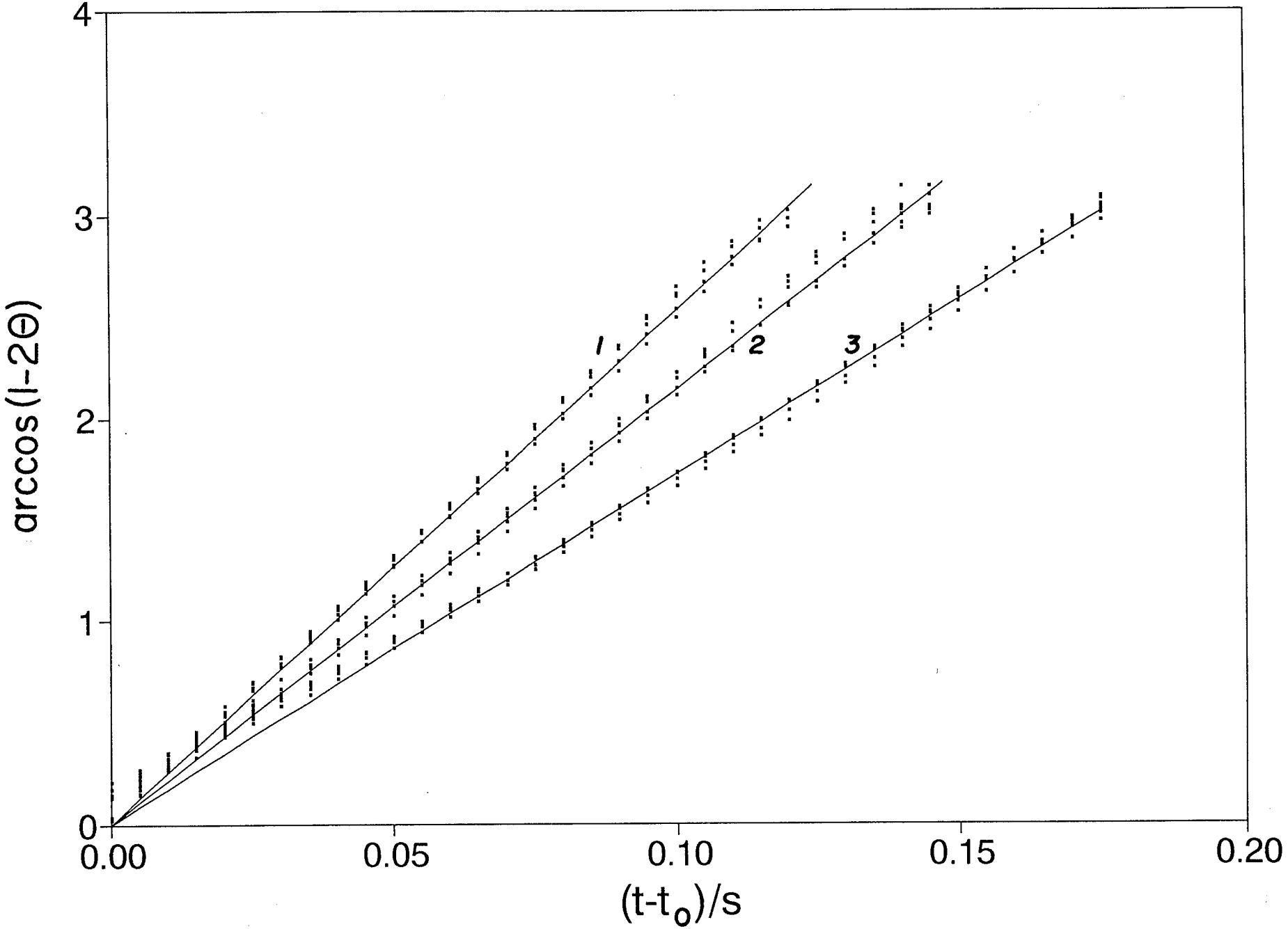

FIG. 4(b)

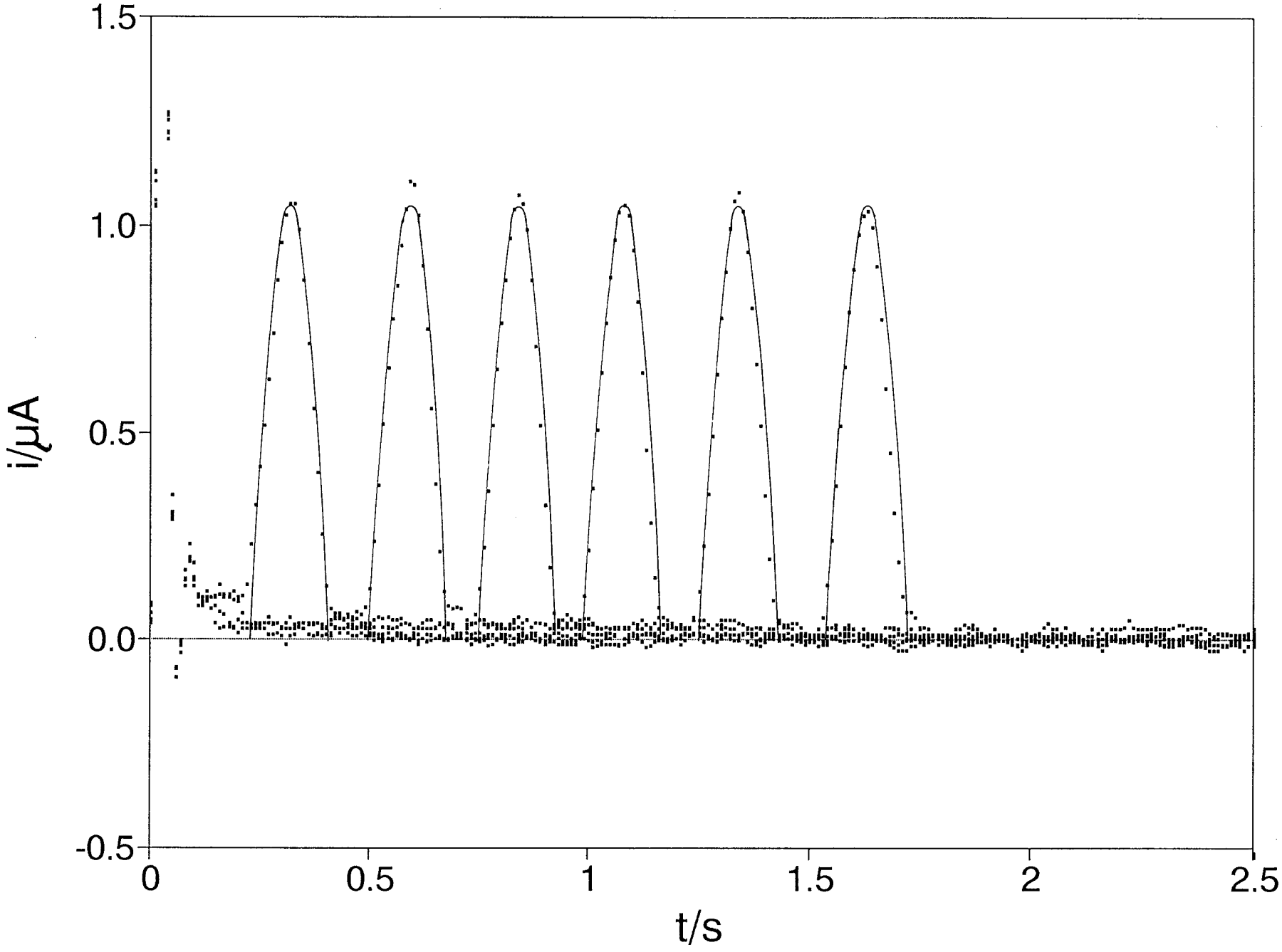

FIG 5

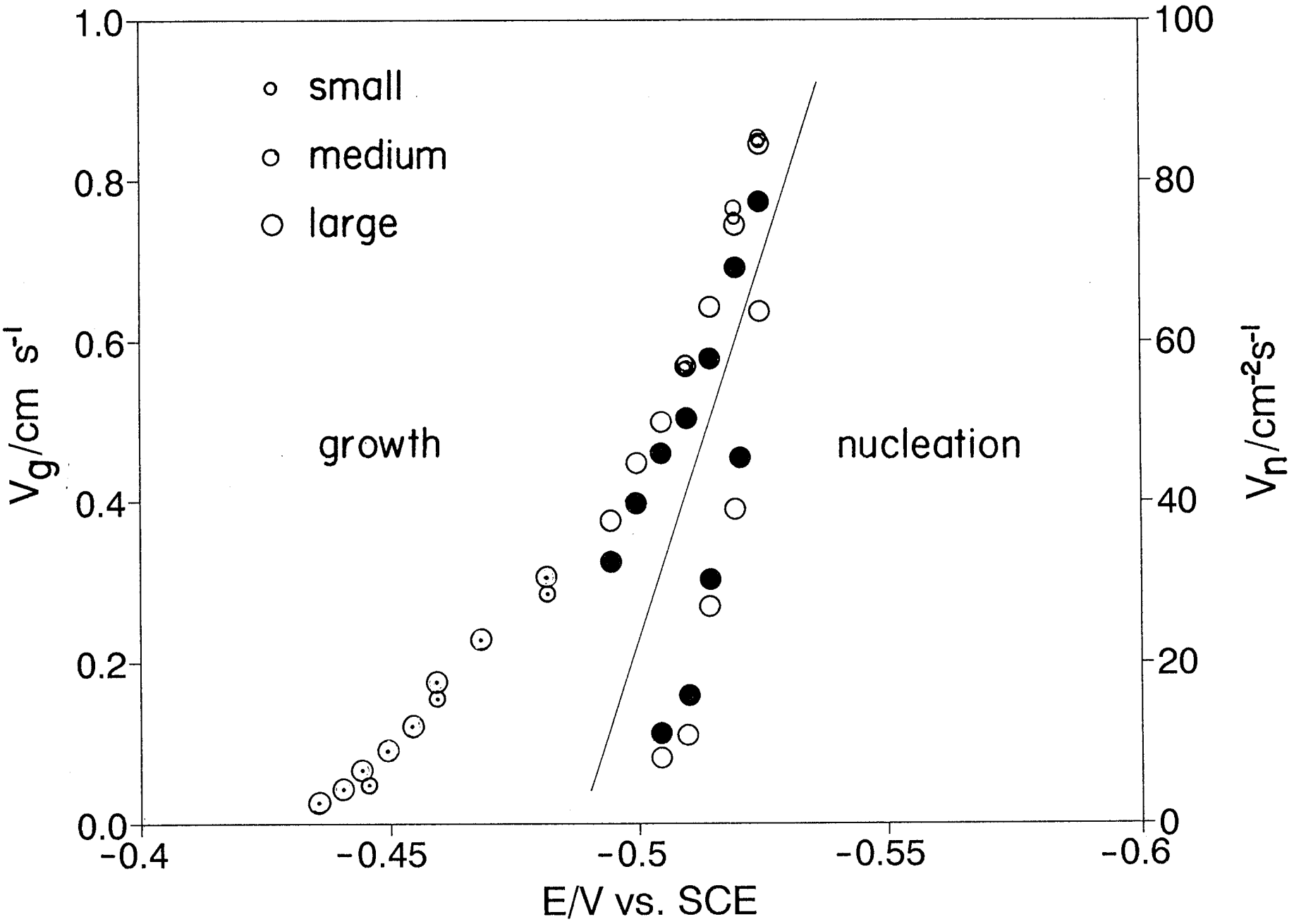
small
medium
large
growth
nucleation
1.0
0.8
0.6
0.4
0.2
0.0
100
80
60
40
20
0
-0.4
-0.45
-0.5
-0.55
-0.6
E/V vs. SCE
V_g/cm s^{-1}
V_n/$cm^{-2}s^{-1}$

FIG. 6

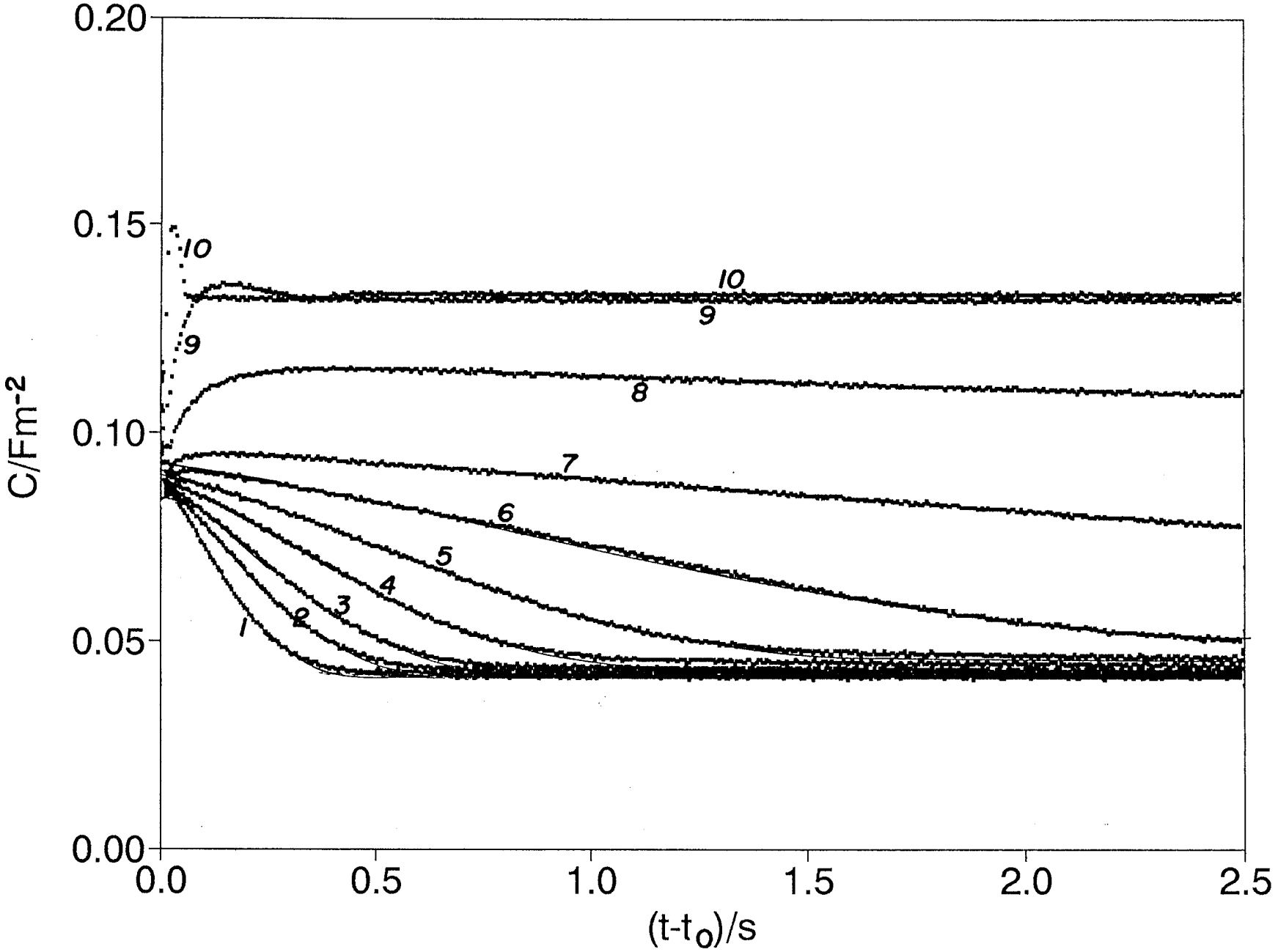

FIG. 7

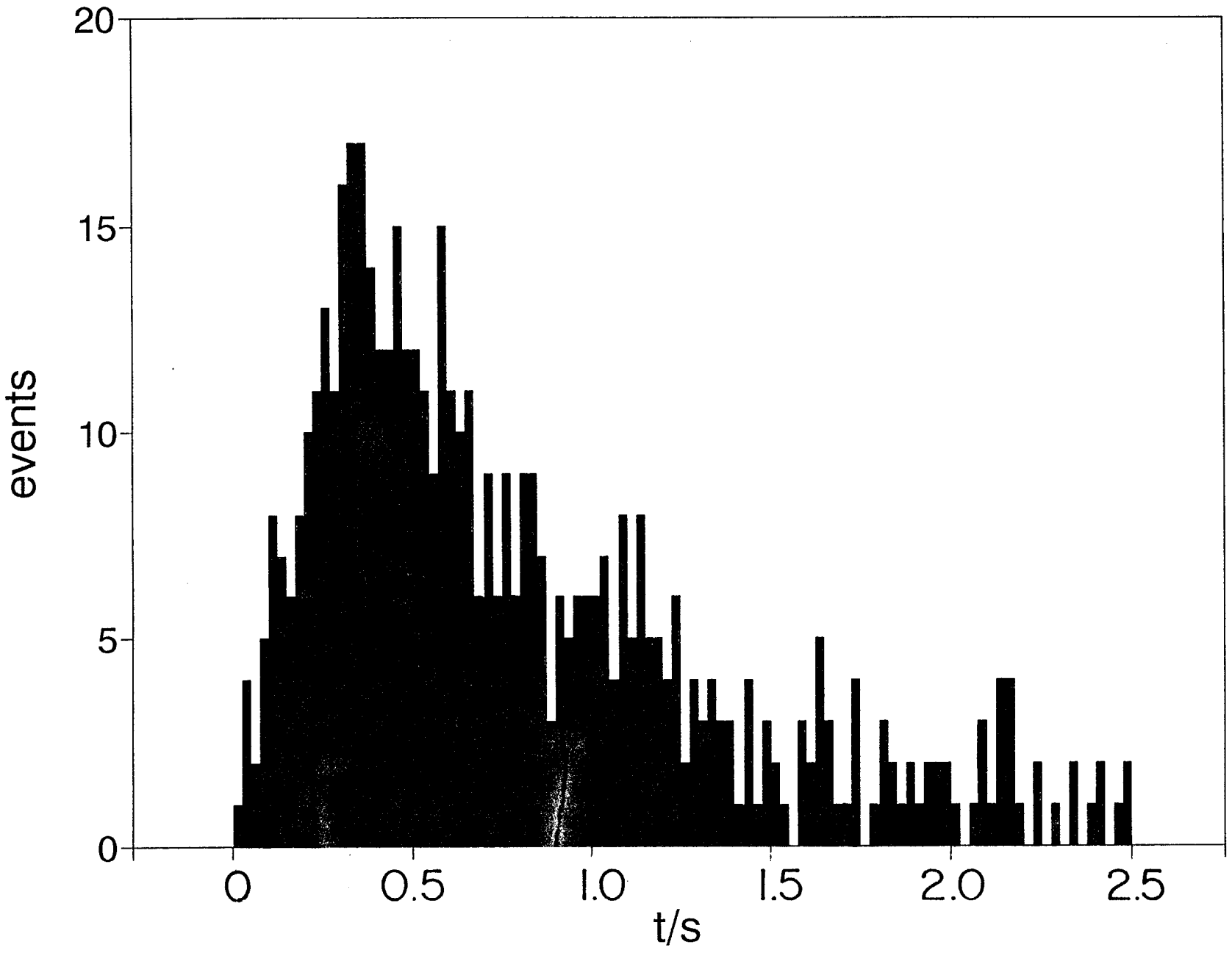

FIG. 8

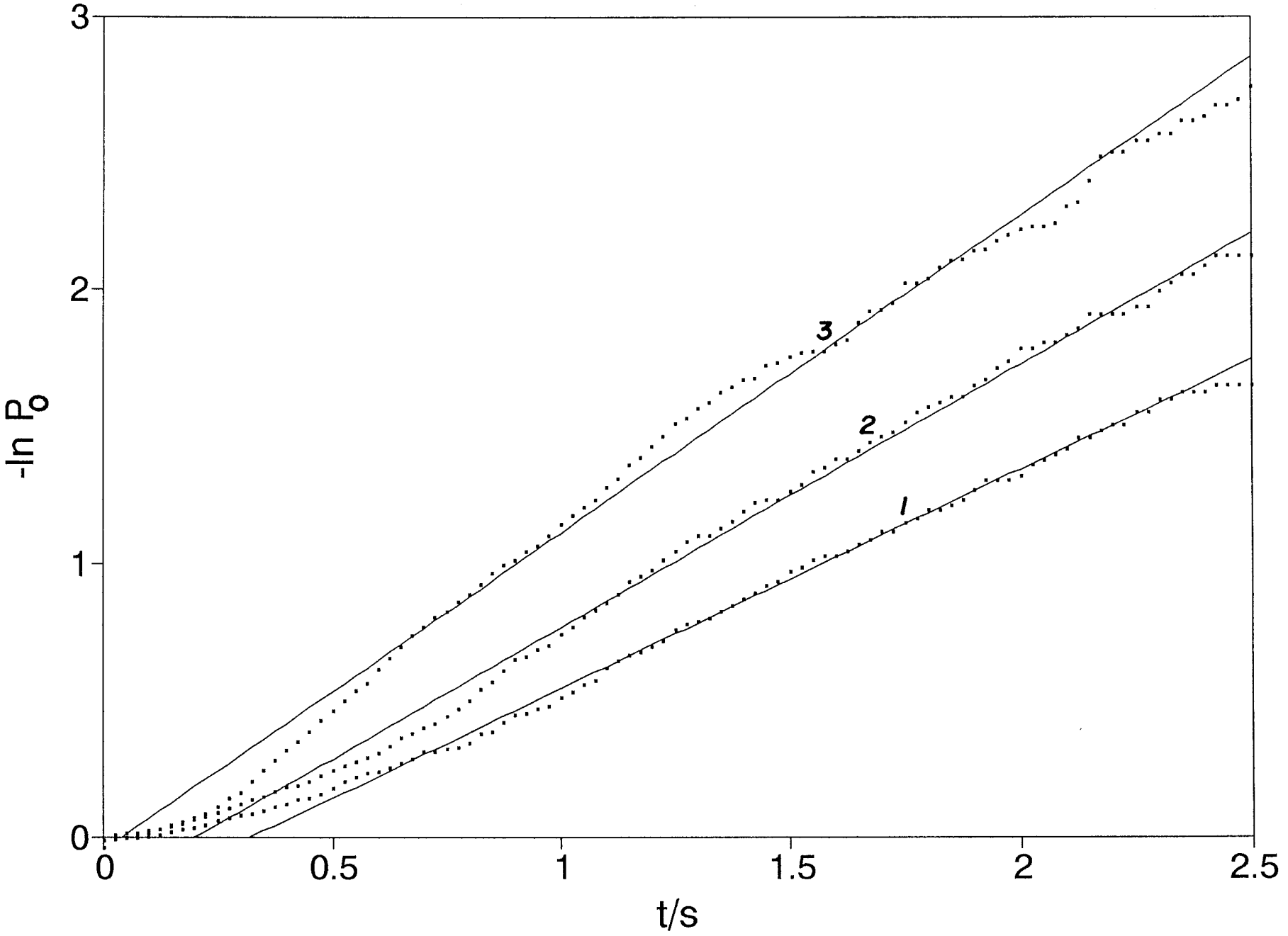

FIG. 9(a)

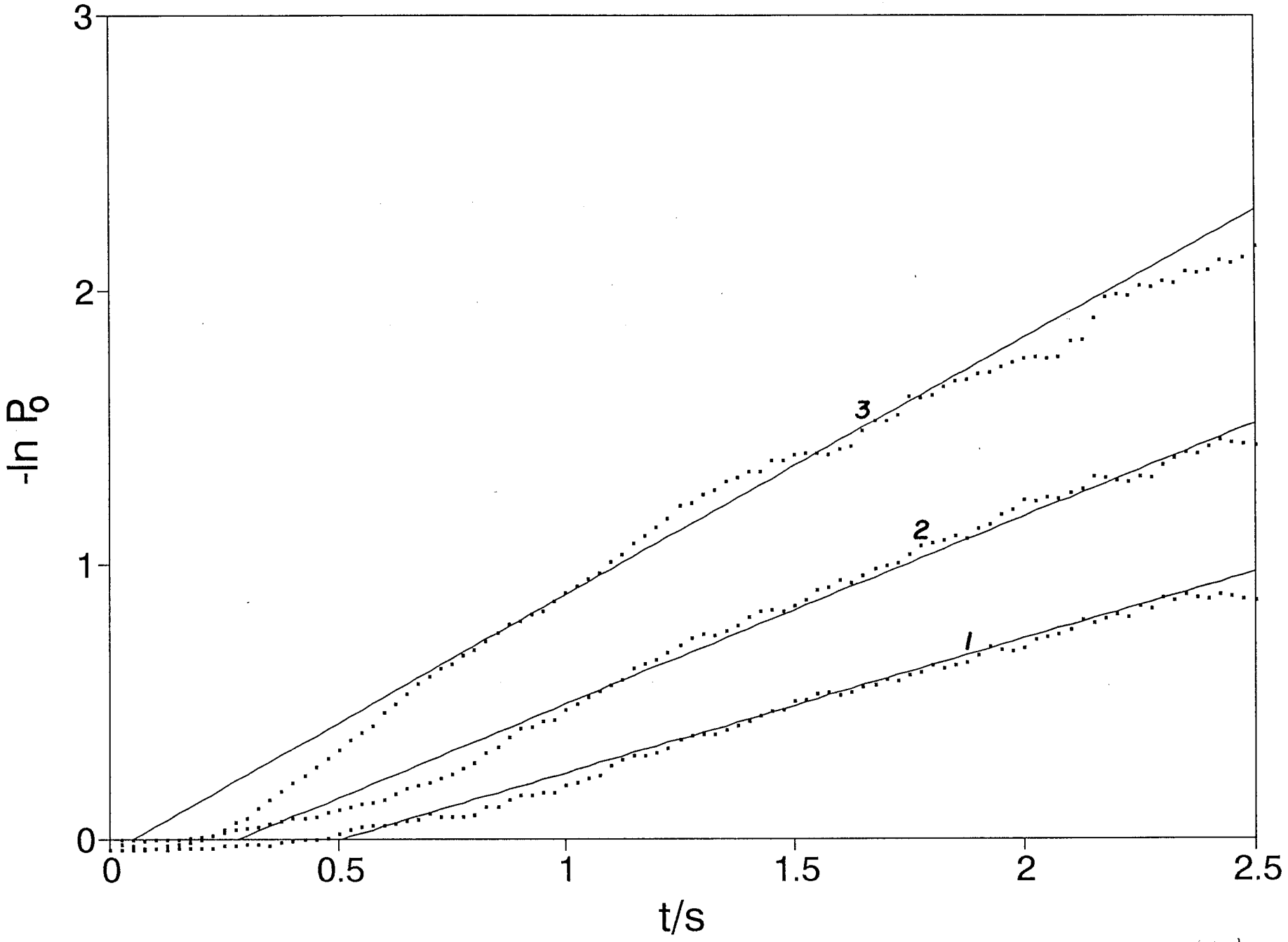

FIG. 9(b)

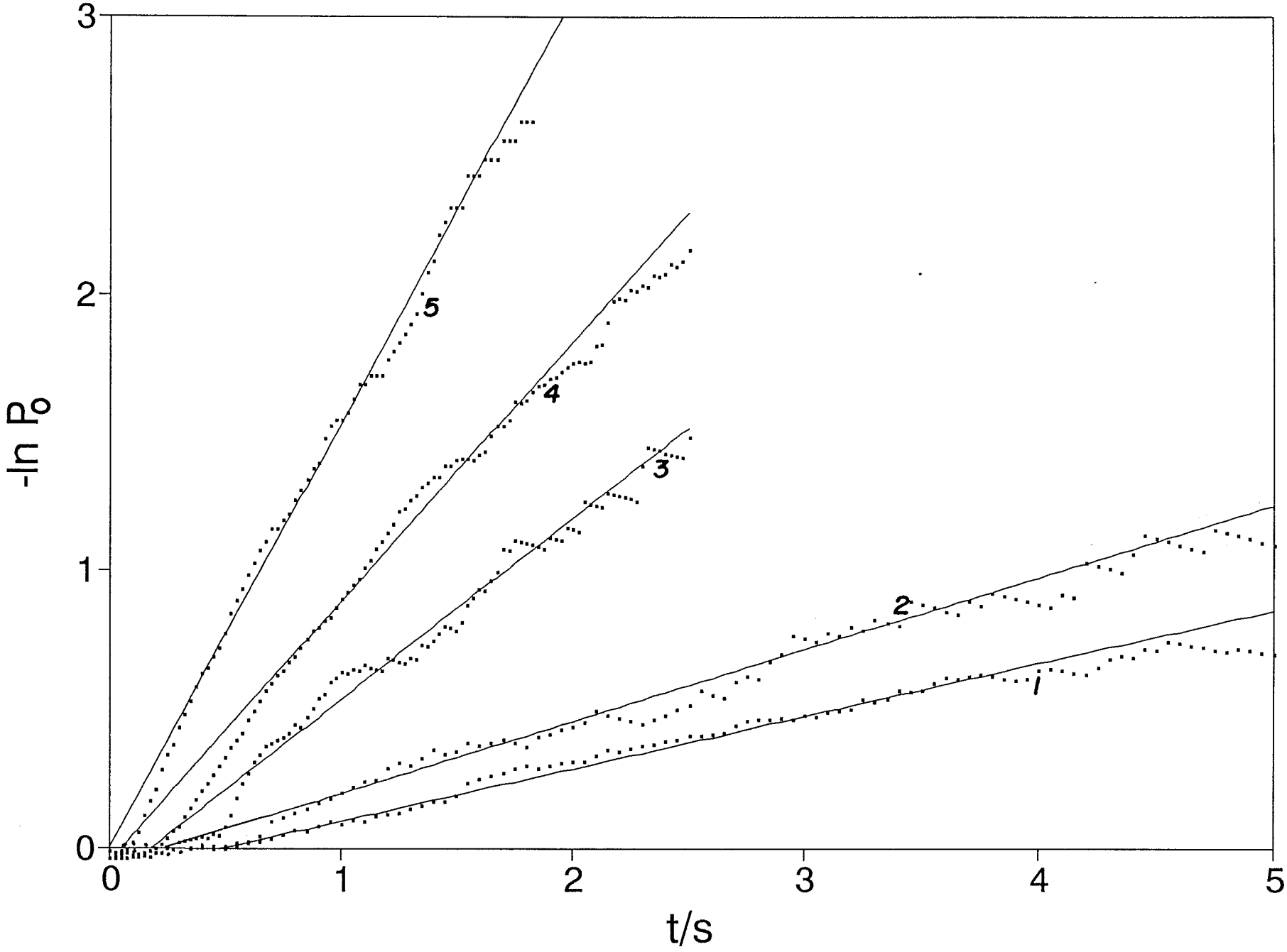

FIG. 9(c)

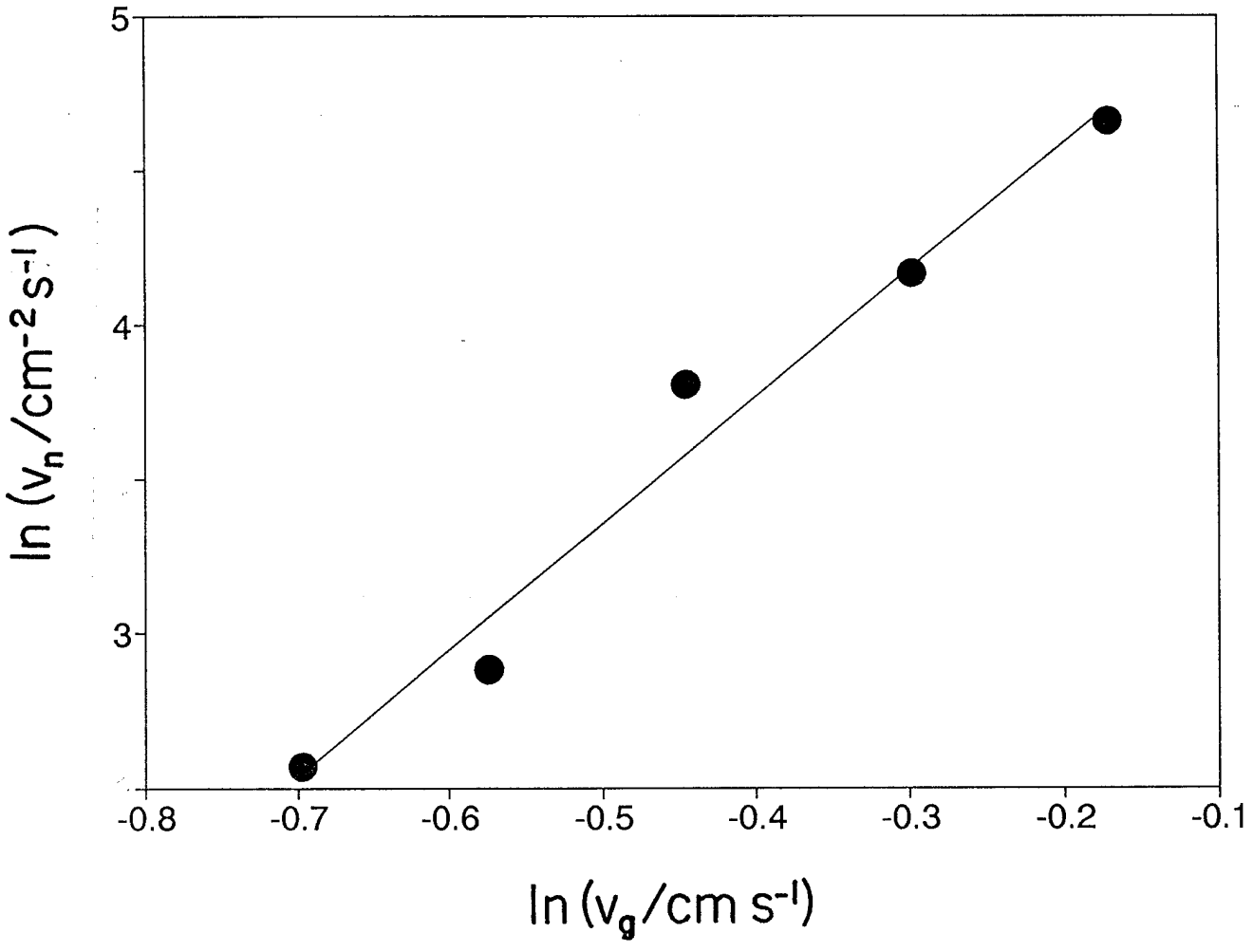

FIG 10

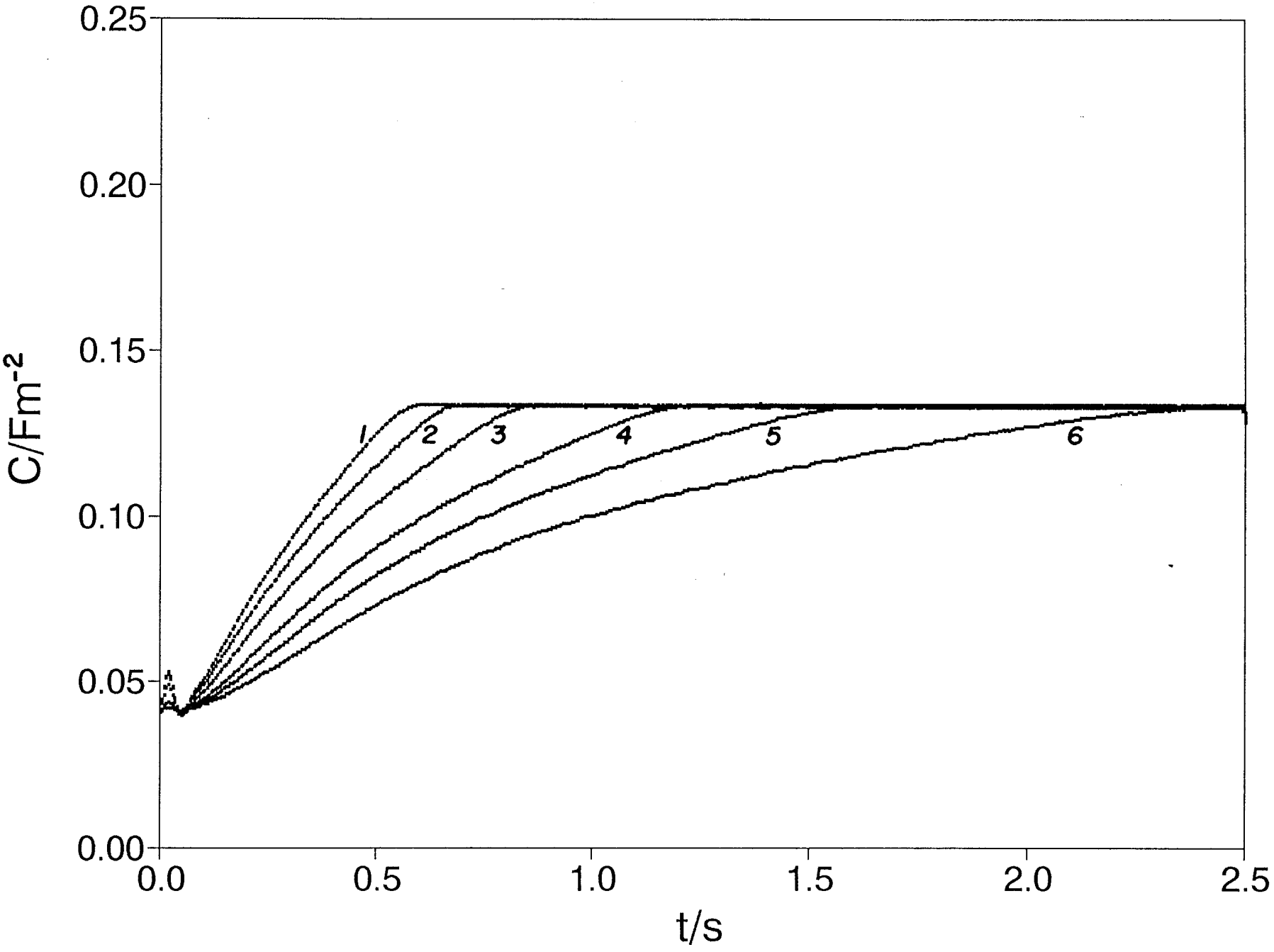

FIG. 11(a).

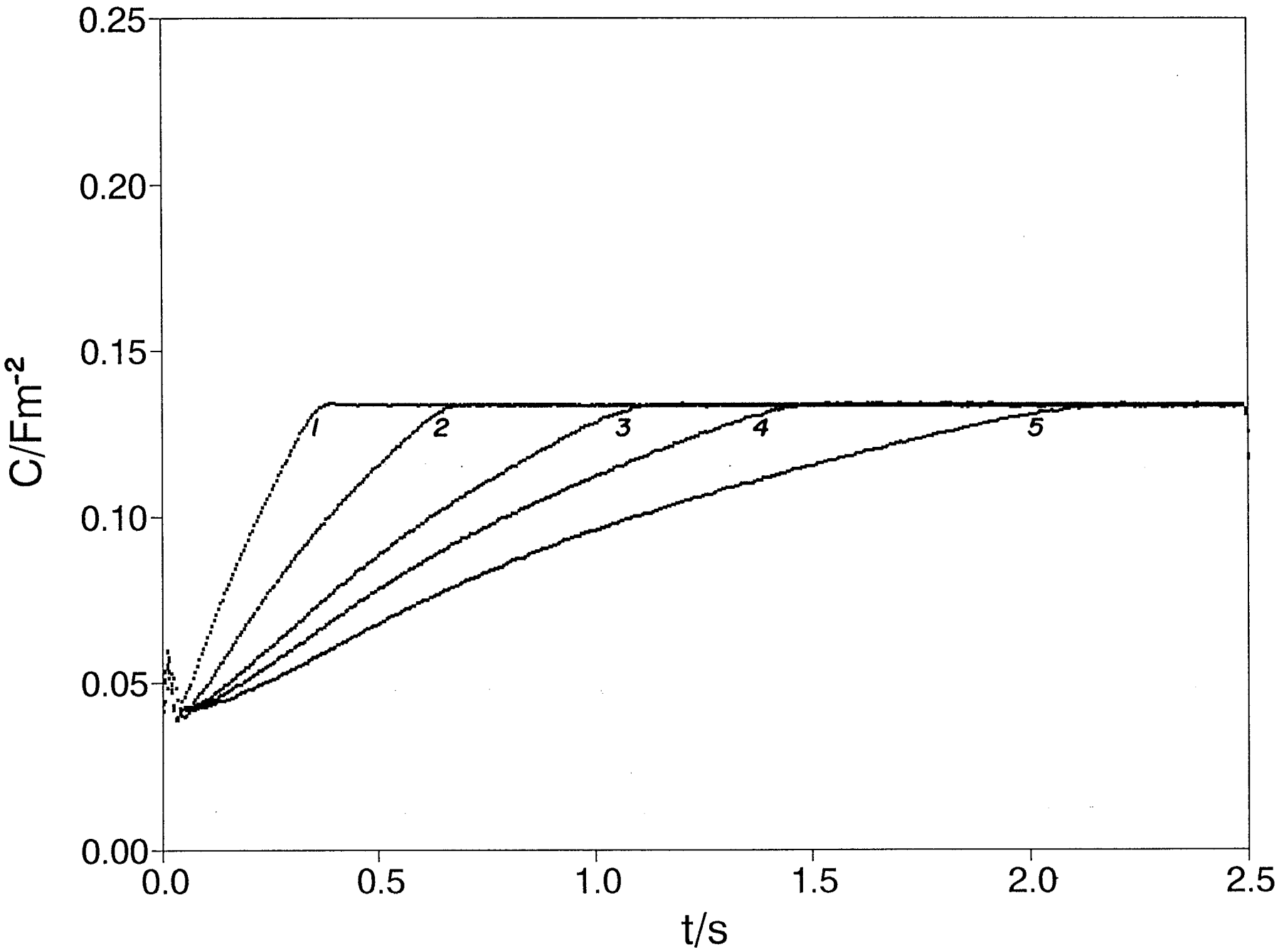

FIG. 11 (b)

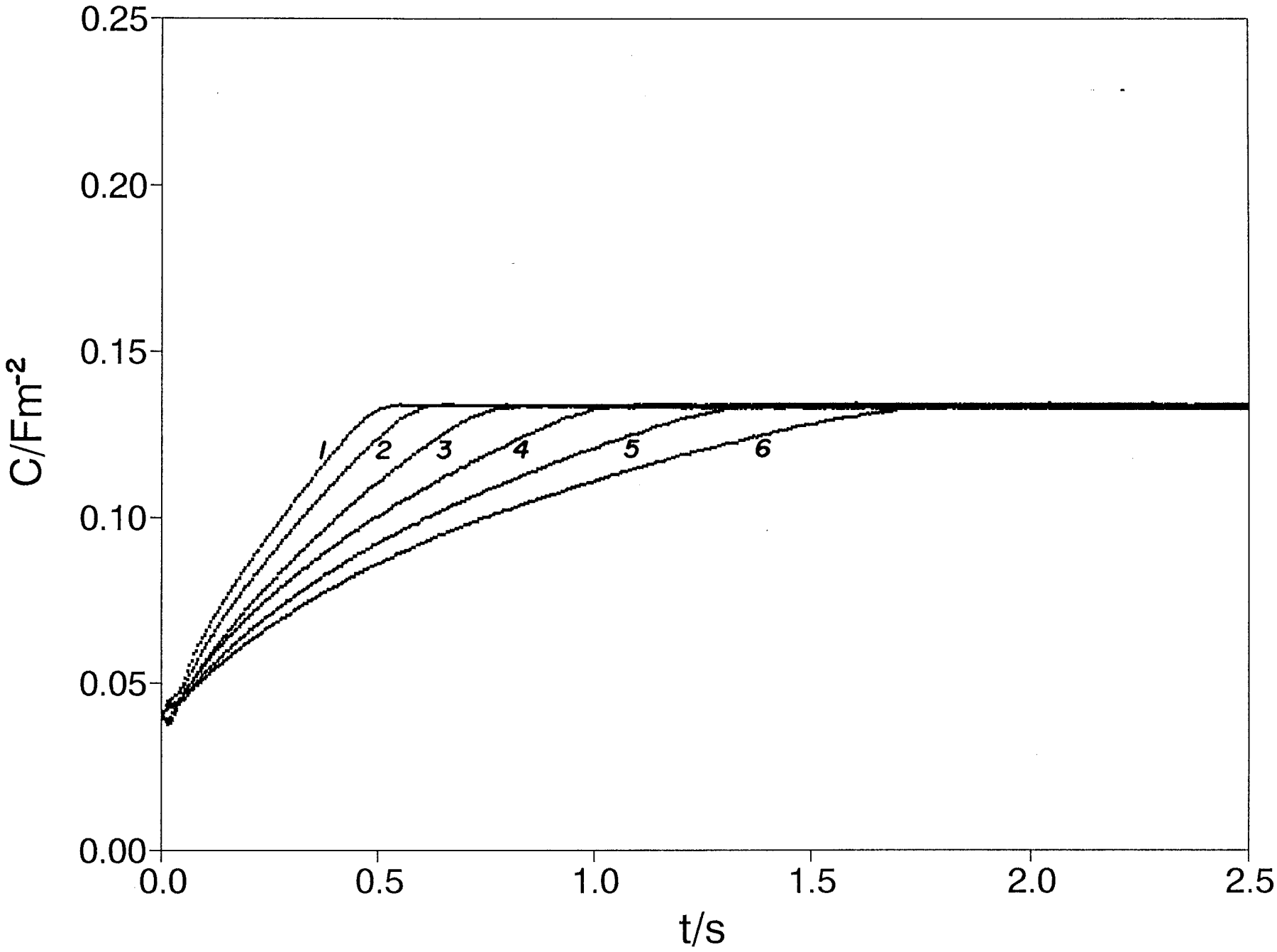

FIG. 12(a)

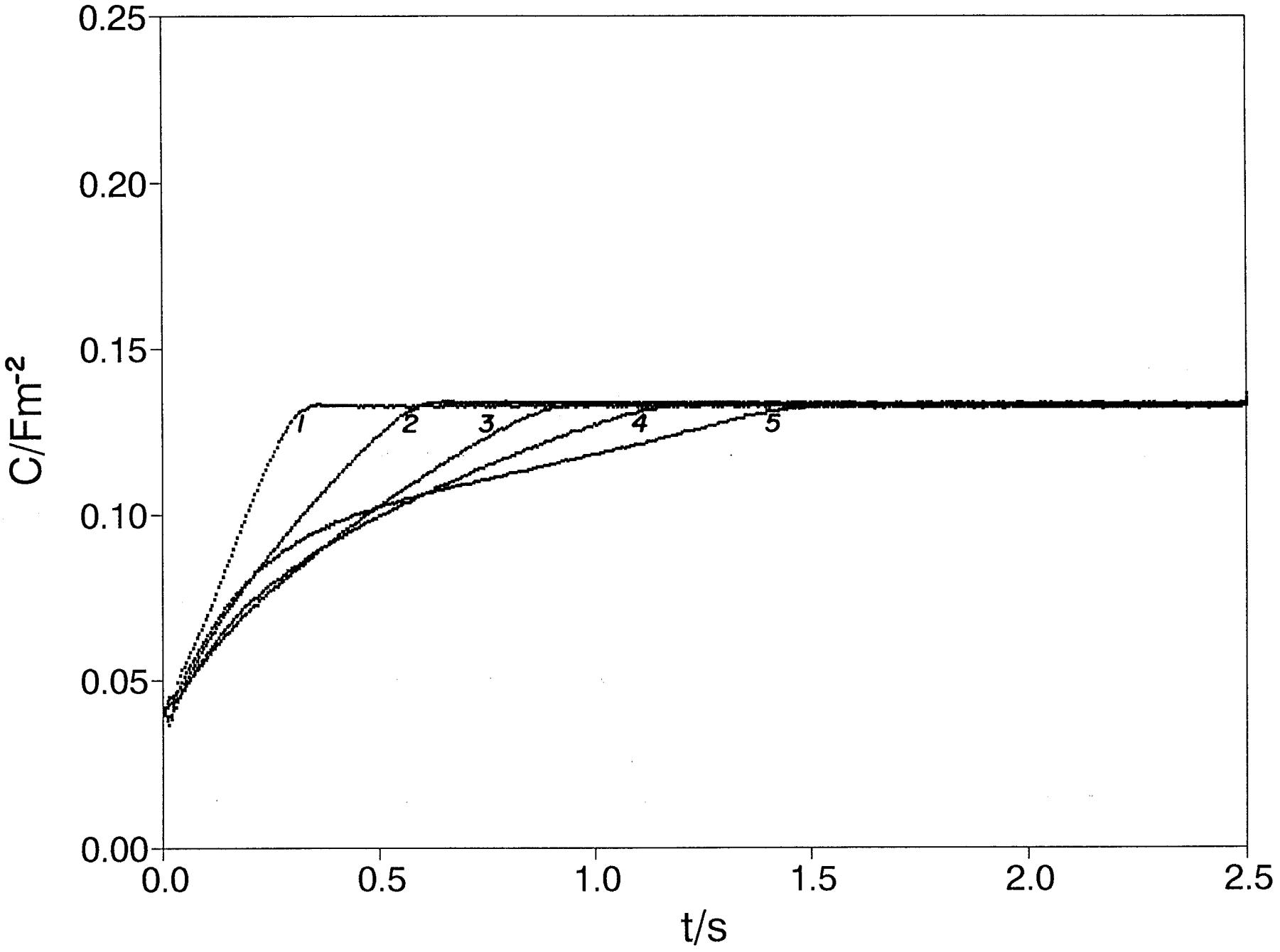

FIG. 12(b)

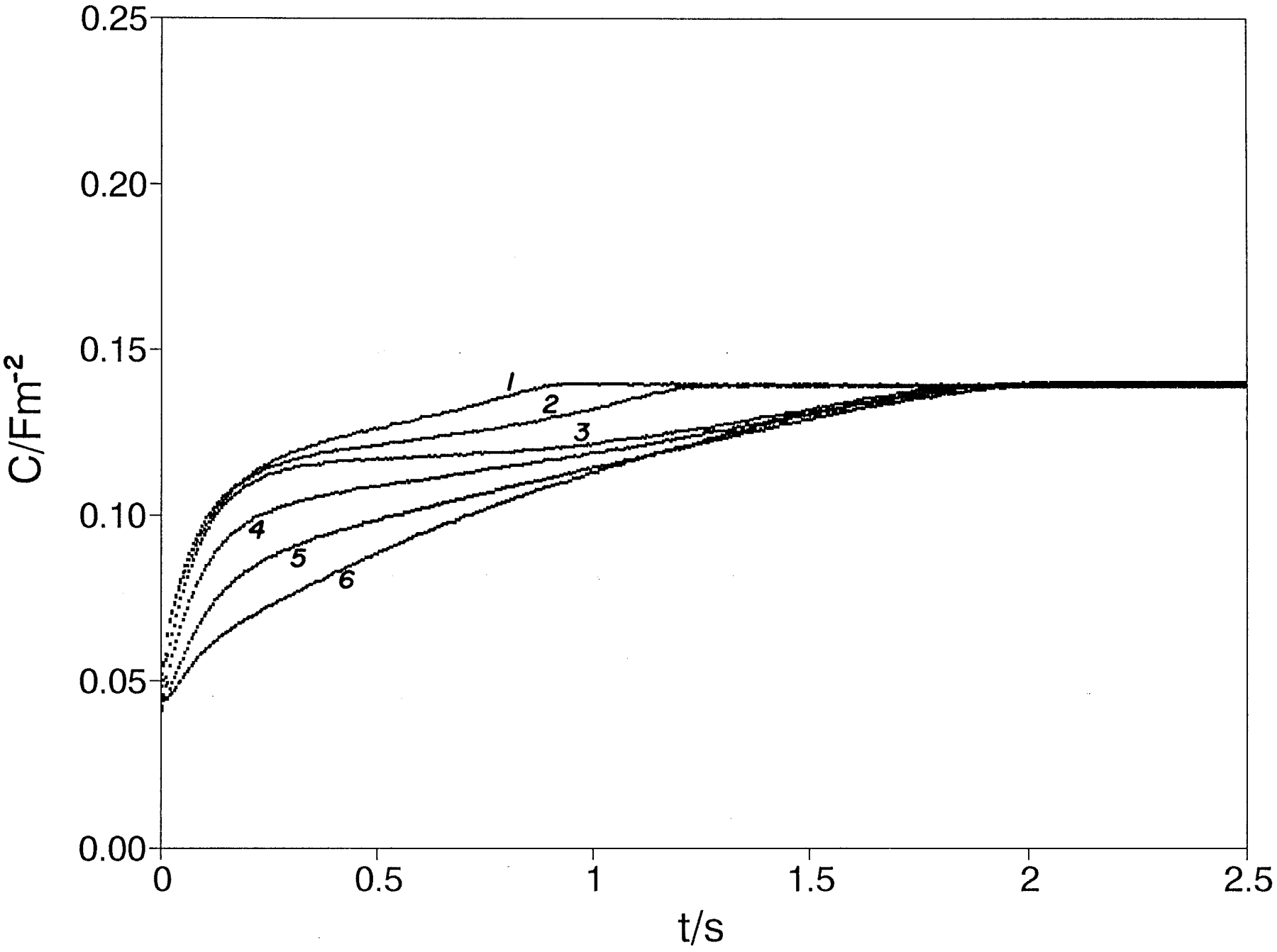

FIG. 13

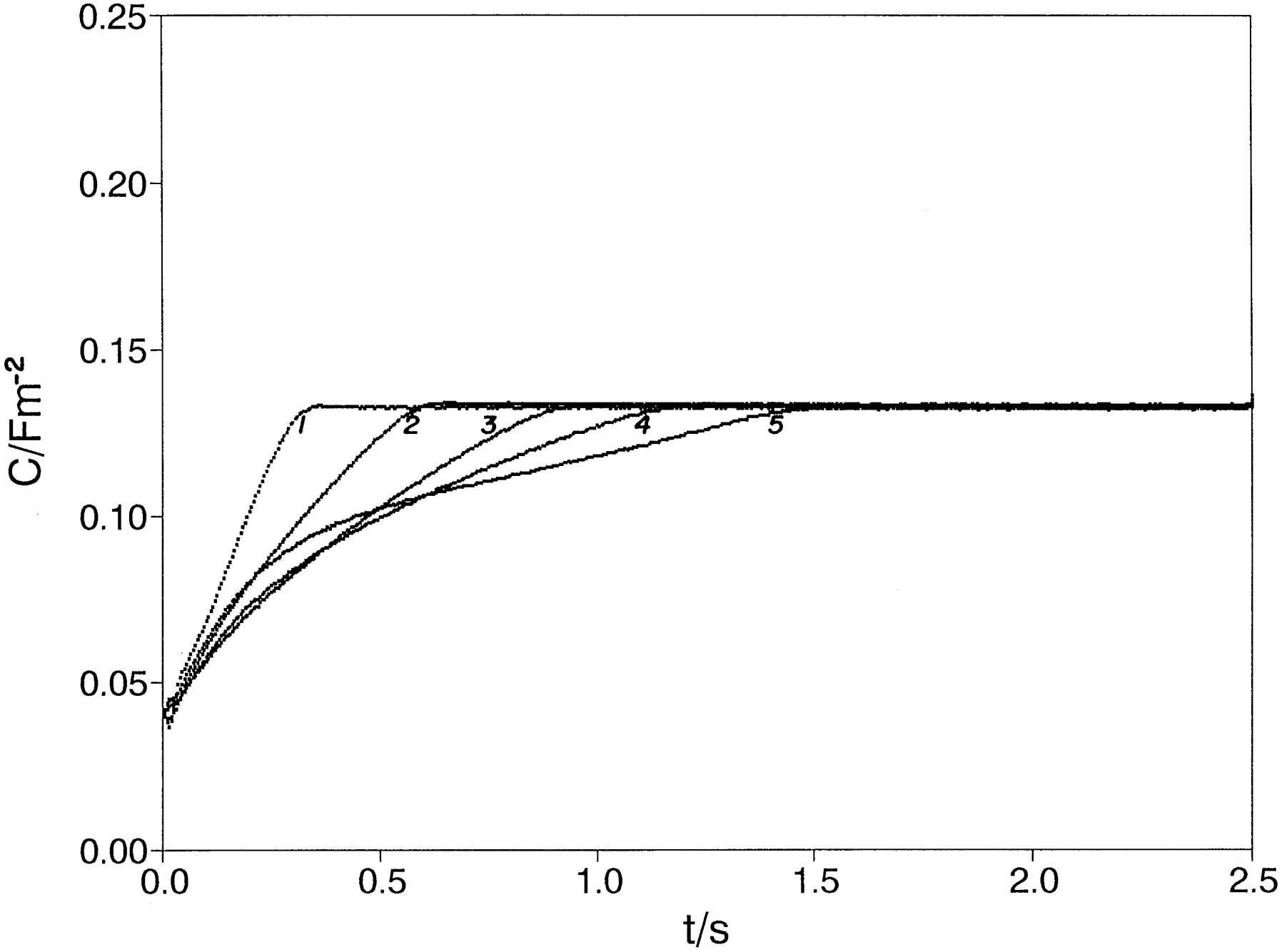

FIG. 12(b)

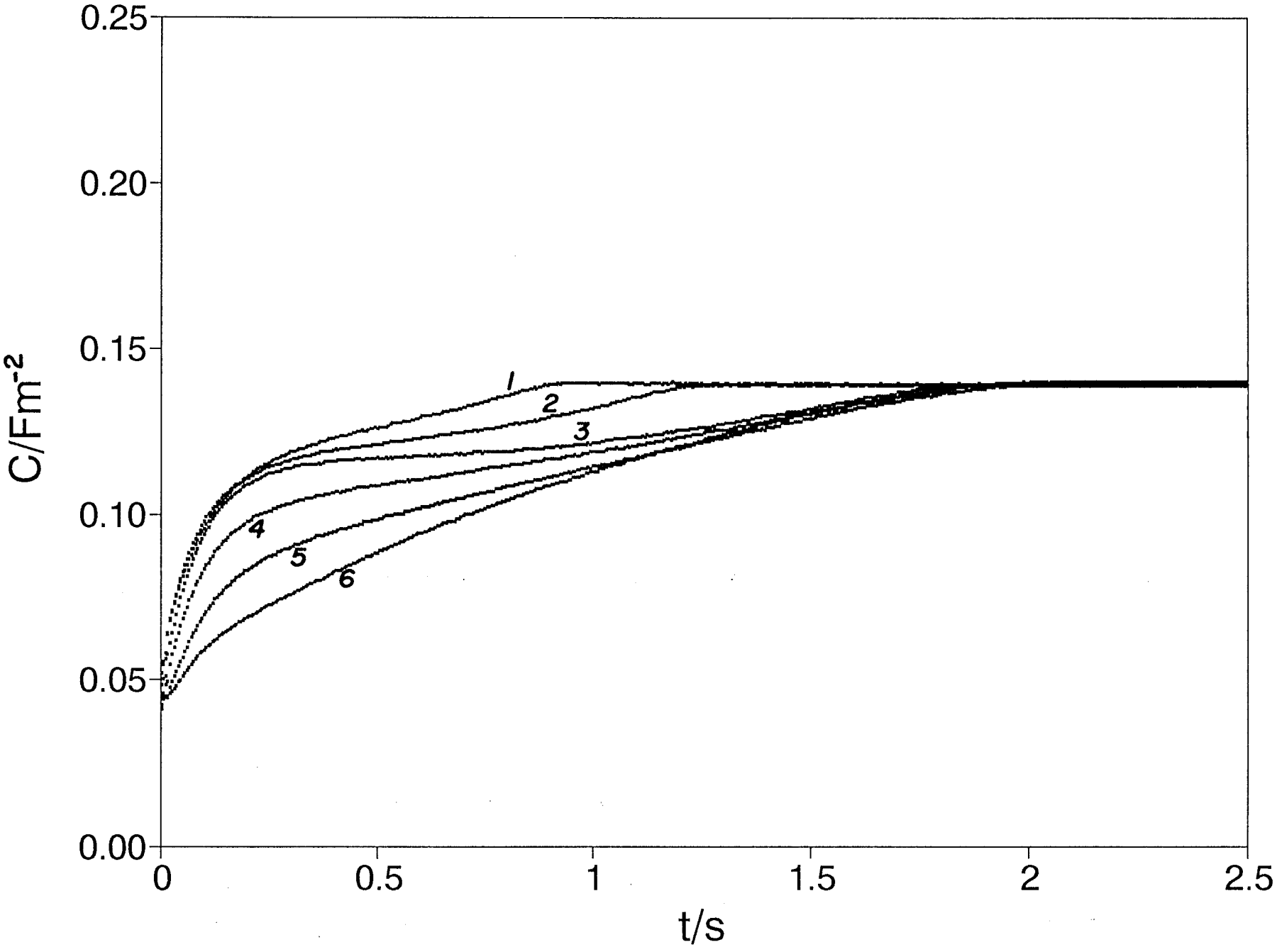

FIG. 13

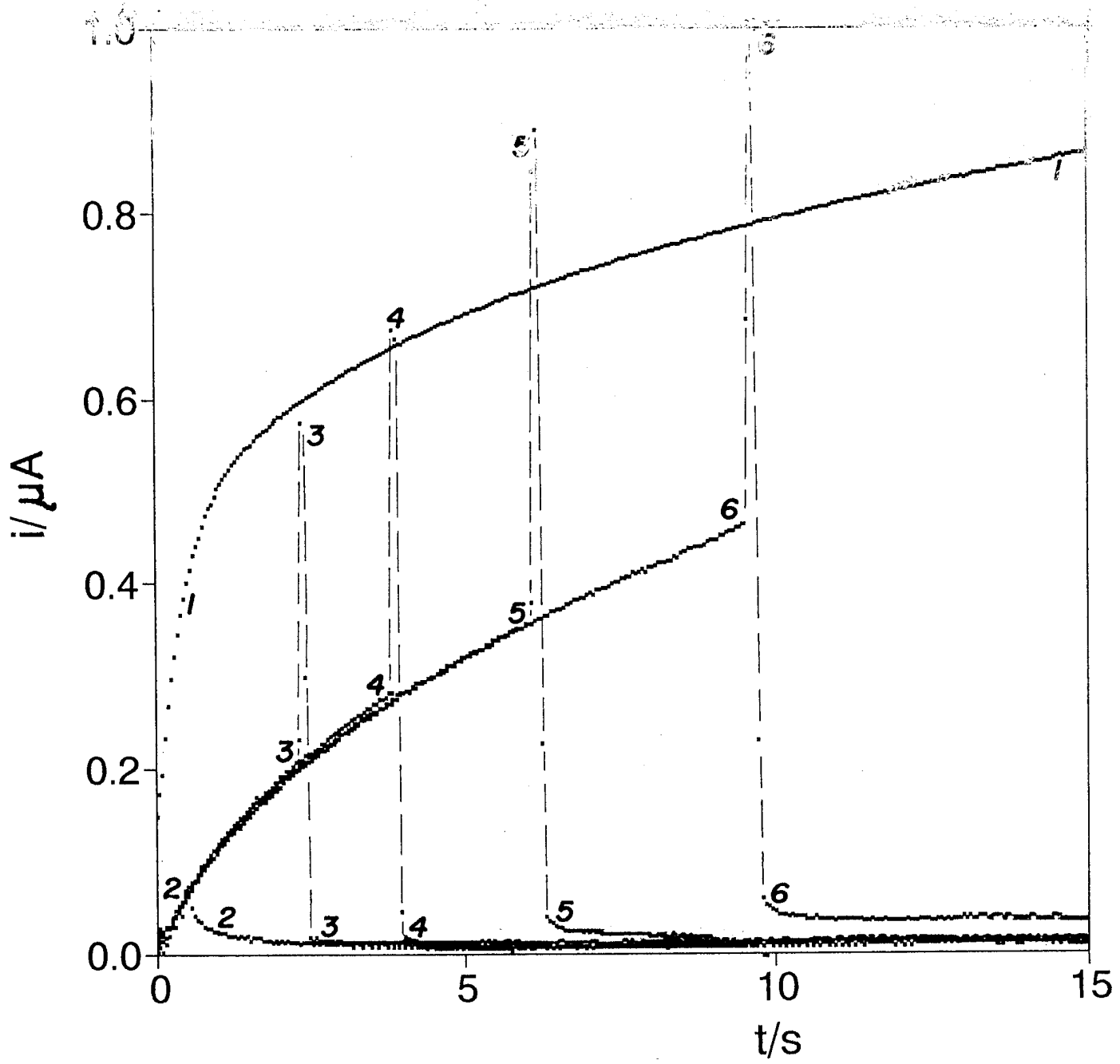

FIG. 14(a)

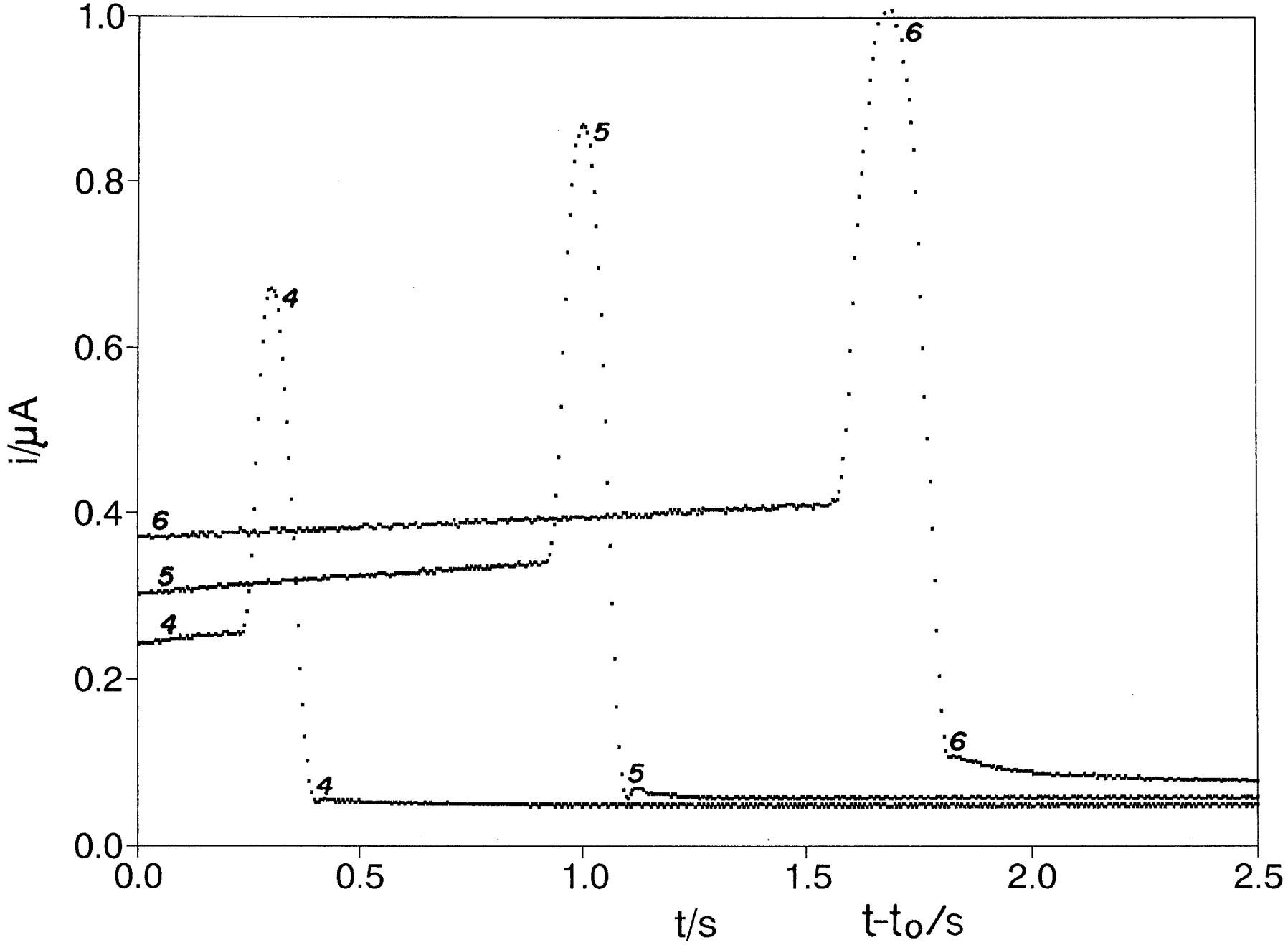

FIG. 14(b)